DESIGN OF DUAL AXIS FORCE SENSOR FOR AEROSPACE APPLICATION

Indikadulla Kankanamge Hasitha Prasanna

(08/9306)

Degree of Master of Science

Department of Electrical Engineering

University of Moratuwa

Sri Lanka

May 2016

DESIGN OF DUAL AXIS FORCE SENSOR FOR AEROSPACE APPLICATION

Indikadulla Kankanamge Hasitha Prasanna

(08/9306)

Thesis submitted in partial fulfilment of the requirements for the degree Master of Science in Industrial Automation

Department of Electrical Engineering

University of Moratuwa

Sri Lanka

May 2016

DECLARATION

I declare that this is my own work and this dissertation does not incorporate without acknowledgement any material previously submitted for a Degree or Diploma in any other University or institute of higher learning and to the best of my knowledge and belief it does not contain any material previously published or written by another person except where the acknowledgement is made in the text.

Also, I hereby grant to University of Moratuwa the non-exclusive right to reproduce and distribute my dissertation, in whole or in part in print, electronic or other medium. I retain the right to use this content in whole or part in future works (such as articles or books).

I K H Prasanna Date:

The above candidate has carried out research for the Masters Dissertation under my supervision.

Prof. Nalin Wickramarachchi Date:

Abstract

This work reports on the design procedure of a dual axis force sensor for aerospace applications. System functionality of the force sensor should comply with many reliability aspects peculiar to aerospace industry rather than just sensing the applied force. Final design of the dual axis force sensor is based on three preliminary design concepts and test data of fabricated models. This report discusses descriptively how to come up with new ideas through these models. Mathematical model of the sensor is used to verify design outcomes. Furthermore this work presents the practical circumstances faced during fabricating and testing. Analysis of results are also discussed in the report and comparison of the first three models included in the report.

Functional requirements were fine tuned in the final design compared to the first three design concepts. Major requirement was to reduce the cross sensitivity when it came to the final design. As desired cross sensitivity was 2% of the applied load, Final design enabled to achieve 2.21% pitch cross sensitivity and 3.84% roll cross sensitivity. It was considerable reduction of the cross sensitivity. Non linearity value was reduced by 65.79% and 38.46% pitch and roll respectively. Achieved non linearity value was 0.065% and 0.08% in pitch and roll direction respectively. Hysteresis also reduced by 73.91% in pitch direction and 21.43% in roll direction.

Output of the Wheatstone bridge has to be reduced in order to decrease the cross sensitivity. This required more amplification, causing the reading and the noises to be amplified at the same time. It was required to have more signal conditioning that was a drawback of the system developed

Acknowledgement

I am heartily thankful to my supervisor, Prof. Nalin Wickramarachchi, whose encouragement, guidance and support from the initial to the final level enabled me to develop an understanding of the subject.

My grateful thanks also go to both Mr. Andy Royal, General Manager, Aero sense technologies (pvt) ltd, United Kingdom, and Mr. Christian Nilsson, Former General Manager, Aero sense technologies (pvt) ltd, Sri Lanka, for giving me permission to conduct internal project as my M.Sc. project, all help me providing all necessary materials and facilities in time and Great ideas and advise throughout the project. This thesis would not have been possible unless my immediate boss Mr. Upul Tennakoon, manager, Technical service center, Aero sense technologies (pvt) ltd, Sri Lanka. He has made available his support in a number of ways. I offer my regards and blessings to all of Aero sense staff who supported me in any aspect during the completion of the project.

Lastly, I should thank many individuals, friends and colleagues who have not been mentioned here personally in making this educational process a success. May be I could not have made it without their supports.

TABLE OF CONTENTS

LIST OF FIGURES

LIST OF TABLES

CHAPTER 1

1. Introduction

This chapter discus about basics of force measurements, the strain gauge functionality and basic types of strain gauge force sensors. Additionally the flight control systems of the commercial air planes, Primary and secondary control surfaces, major flight control systems and control devices in the cock pit are described. Major differences of them and mechanisms are also discussed.

1.1 Force measurement

Force measurement is a crucial event in most of the control systems. Now a days it has developed in many aspects and vast verity of transducers have been developed. Applications of the force transducers are also been developed in parallel, from simple industrial weighing application to the finger tip of the robot arm which sense the touch of the objects. Most of the force transducers are function according to two basic concepts. 1. Piezoresistive effect is the electrical resistance changes when material is mechanically deformed. 2. Piezoelectric effect is the generation of electric charge by a crystalline material upon subjecting it to stress [1]. Additionally MEMS capacitive sensors are also popular in many industries such as robotics and biological experiments. Capacitive force sensors, very small deflections caused by applied forces are transduced into detectable capacitance changes. Capacitive sensors are capable of measure forces from mN (10−3 newton) to pN (10−12 newton) [2]. Capacitive sensors usually have disadvantages such as severe hysteresis and temperature sensitivity. On the other hand, capacitive sensors have the advantage of the availability of small sized, and high sensitivity [2,3].

Silicon piezoresistive sensors are commercially used in verity of force measurement applications and also known as semiconductor strain gauges. The effect of stress on doped silicon and germanium has been known since 1954 and since then, researchers have extensively reported on micro scale, piezoresistive strain gauges, pressure sensors, accelerometers, and cantilever force-displacement sensors, including many commercially successful devices [4]. Metallic foil strain gauges are also a type of piezoresistive sensor. Depending on the application of force measurement the strain gauge can be either metallic of semiconductor strain gauges. Semiconductor strain gauges are very small and have large gauge factor. In fact, resistance change due to the strain is much bigger that the metallic strain gauges. On the other hand metallic

strain gages have higher linearity over resistance change on applied strain comparted to the semiconductor strain gauges. [5].

Lead zirconate titanate (PZT) is one of the known piezoelectric material used in many force measurement applications. PZT Forces sensor can be considered as a breakthrough of design of the scanning force microscope [6].

1.2 Mettle foil strain gauge based force sensors

1.2.1 Mettle foil strain gauges

The strain gauge has been in use for many years and is the fundamental sensing element for many types of sensors, including pressure sensors, load cells, torque sensors, position sensors, etc. metal Foil type strain gauges are available in a wide verity of shapes and sizes to suite with various applications. They consist of a pattern of resistive foil named as grid which is mounted on a backing material. The most common foil materials are alloys constantan, nichrome, advance, and karma. Typical resistances vary from 100 ohms to several thousand ohms to possess good sensitivity [1]. Two ends of the resistive foil connected to the solder tabs which are used to wire the gauge. In addition to those four alignment marks are placed align to the center line of the grid area. Figure 1.1 shows the basic parts of the strain gauge.

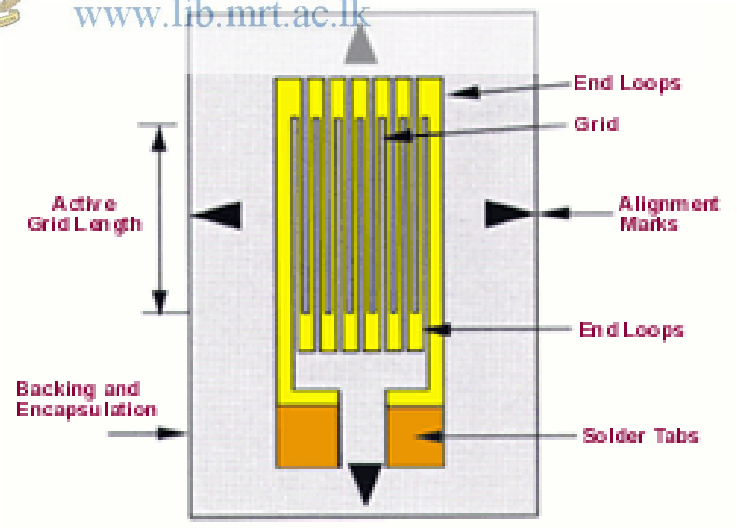

Figure 1.1: Basic parts of the strain gauge.

When a strip of conductive metal is stretched, it will become thinner and longer, both changes resulting in an increase of electrical resistance end-to-end. Conversely, if a strip of conductive metal is subjected to the compressive force it will broaden and

shorten, result is decrease in resistance. If these stresses are kept within the elastic limit of the metal strip does not permanently deform. Change of resistance of the strip can be used as a measurement of strain and it can relate to the applied load. Same concept applies in strain gauge, it deforms with the material which subjected to the force and make the changes in the resistance of grid.

1.2.2 Strain gauge base force sensors

Strain gauge based force sensors are generally named as load cells. They are basically consisting with metal structure which elastically deforms when subjected to a force and strain gauges which are pasted on the structure and deforms with it. Load cells are divided in to two main categories based on the geometry of them, called beam type load cell and ring type load cell [7]. Other than that load cells are categories based on type of stress developed on the measuring element, called bending load cells and shear load cells.

A vast number of load cell types have been developing over the past years. Bending beam, shear beam rectangular, shear beam round, miniature, Low profile, ‘S’ of ‘Z’ beam, canister, ring, button and single point load cells [5],[8].

The 'S' or 'Z' Beam Load Cell

A simple design of load cell, structure of the load cell is shaped as a 'S' or 'Z' and strain gauges are bonded to the central sensing area. Figure 1.2(a) shows an example of S or Z type load cell.

The Bending Beam Load Cell

The strain gauges are bonded on the flat upper and lower sections of the load cell at points of maximum strain. This load cell type is used for low capacities and performs with good linearity. Its disadvantage is that it must be loaded correctly to obtain consistent results. Figure 1.2 (b) shows an example of bending beam load cell.

Shear load cell

Strain gauge-based load cell structures, configured to operate based upon the measurement of shear strain, provide high capacity and low compliance in a compact and low profile geometry.

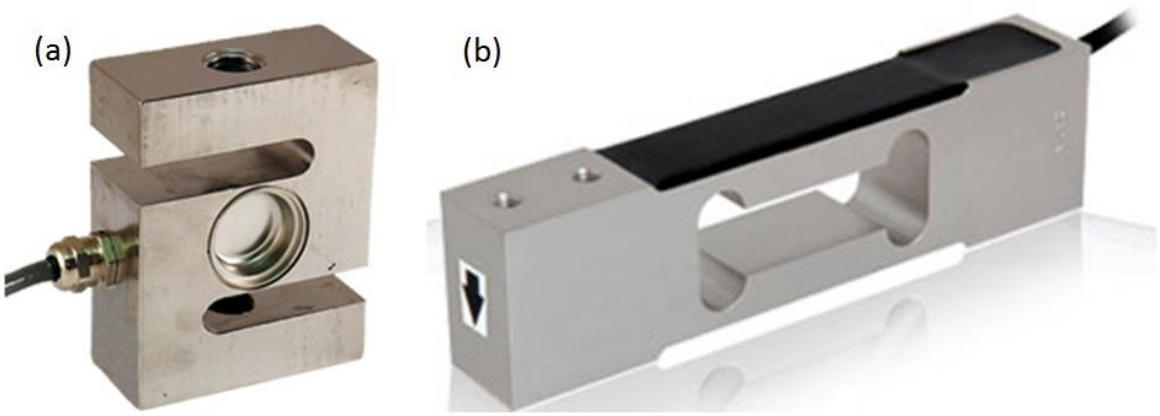

Figure 1.2: Example of load cells

1.3 Flight Controls

A conventional fixed-wing aircraft flight control system consists of basic three parts in order to control an aircraft's direction in flight. Rotations around the basic three axes of the flight are controlled by the flight controls surfaces, respective cockpit control devices of control surfaces, and the necessary operating mechanisms in between the cockpit control devices and control surfaces. Aircraft engine controls are also considered as flight controls.

1.3.1 Axes of rotations

An airplane basically turns around imaginary three axes with respect to the ground or other fixed object. All three axes intersect at the center of gravity of the airplane and each one is perpendicular to the other two.

Longitudinal axis runs from nose to tail of the airplane. Rotation around the longitudinal axis is called roll. So, longitudinal axis is called axis of roll as well. The lateral axis passes through an aircraft from right wingtip to left wingtip. Rotation around lateral axis is called pitch. Same way it is called Axis of pitch. Other axis runs from top to bottom of the aircraft vertically. So it is called vertical axis and the same time it is called axis of yaw, rotation around the vertical axis is called yaw [9]. Figure 1.3 illustrates the axis of rotation of an airplane.

1.3.2 Control surfaces

The main control surfaces of an aircraft control the main three rotations of the aircraft around the three axes of rotation. Those are attached to the airframe on hinges or tracks. While they are moving, they deflect the air stream passing over

them. Deflection of the air stream generates an unbalanced force to rotate the aircraft about the associated axis. The fixed-wing aircrafts have three main control surfaces [10], [11]. Figure 1.4 shows the placement of main control surfaces of the airplane

- Ailerons -

The ailerons control the airplane's roll about its longitudinal axis. Ailerons are mounted on the trailing edge of each wing near the wingtips, and move in opposite directions. While one aileron goes up other aileron goes down. A raised aileron reduces lift on that wing and a lowered one increases lift. This causes the aircraft to roll about its longitudinal axis.

- Elevator -

An elevators are mounted on the trailing edge of the horizontal stabilizer on each side of the fin in the tail. Both elevators move up and down together. While moving elevators they control the airplane's pitch about its lateral axis. When the elevators go up, raised elevators push down on the tail and cause the nose to pitch up. This makes the wings fly at a higher angle of attack which generates more lift and more drag.

- Rudder -

The rudder is typically mounted on the trailing edge of the fin. Rudder moves left and right. Deflecting the rudder right pushes the tail left and causes the nose to yaw to the right. Centering the rudder pedals returns the rudder to neutral and stops the yaw. Obviously rudder controls the yaw of airplane around its vertical axis.

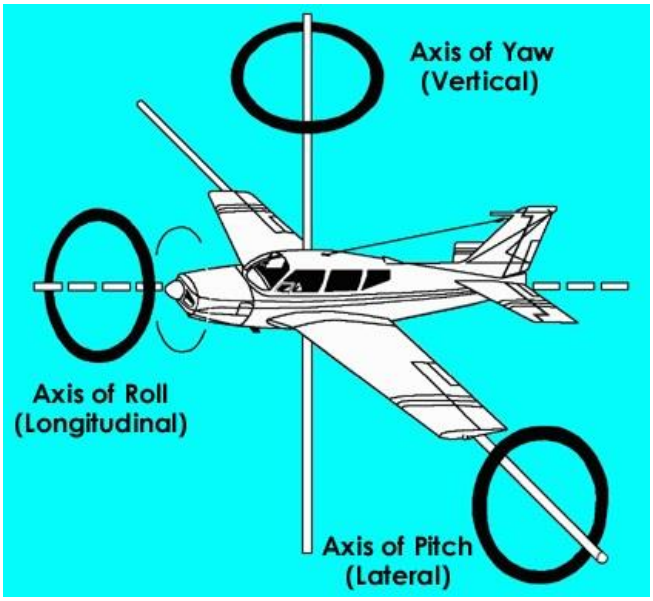

Figure 1.3: Main axis of rotation of the airplane

In addition to the main control surfaces airplane consists of few secondary control surfaces. Few of them allow pilot to do fine adjustment of main controls and rest do control some other aspect.

- Spoilers -

Spoilers are used to disrupt airflow over the wing and greatly increase the amount of drag. This allows pilot to lose altitude without gaining excessive airspeed. Spoilers are sometimes called "lift dumpers".

- Flaps -

Flaps are mounted on the trailing edge of each wing. They are deflected down to increase the effective curvature of the wing. They are used during low speed, high angle of attack flight including take-off and descent for landing.

- Slats -

Slats are mounted on leading edge of the wing. They are extended to the front of a wing and altering the airflow over the wings and intended to reduce the stalling speed for take-off and landing.

- Trim Tabs -

A trim tab is a small, adjustable hinged surface on the trailing edge of the aileron, rudder, or elevator control surfaces. Trim tabs are enabling the pilot to release manual pressure on the primary controls. Some airplanes have trim tabs on all three control surfaces that are adjustable from the cockpit, others have them only on the elevator and rudder; and some have them only on the elevator. Some trim tabs are the ground-adjustable type only. The tab is moved in the direction opposite that of the primary control surface, to relieve pressure on the control wheel or rudder control.

1.3.3 Cockpit Control Devices

Most common flight control devices are yoke, Center stick and side stick. All of them are pitch and roll controllers of aircrafts.

Yoke is used to control the attitude of the airplane and shown in the Figure 1.5(a). Rotating the yoke controls the ailerons and the roll axis. Push and pull movement of the yoke controls the elevator and the pitch axis. Yokes come in a variety of shapes and sizes, the most common being of a "U" or "W" design. Some aircraft use an "M" style. There are some rarer styles, such as circular designs much like a steering wheel. Yokes are less sensitive and allow to a larger range of motion and provide more visual feedback to the pilot. Yokes take up more room than side sticks in the cockpit.

A center stick is an aircraft control column, which is located conventionally in the center of the cockpit between the pilot's legs as shown in Figure 1.5(b). The center stick is used in many military fighter jets and in light aircrafts

A side-stick is located to the side of the pilot, usually at the right or outboard on a two-seat flight deck as shown in Figure 1.5(c). The side-stick is used in many modern military fast jets.

Major control devices can be divided in to two categories as Primary control devices and secondary control devices.

1.3.3.1 Primary controls.

A control column or a control yoke controls roll and pitch of the airplane , which moves the ailerons when turned or deflected left and right, and moves the elevators when moved backwards or forwards

Rudder pedals to control yaw, which move the rudder. Left foot forward will move the rudder left for instance airplane yow to the left side.

Throttle controls to control engine speed or thrust for powered aircraft.

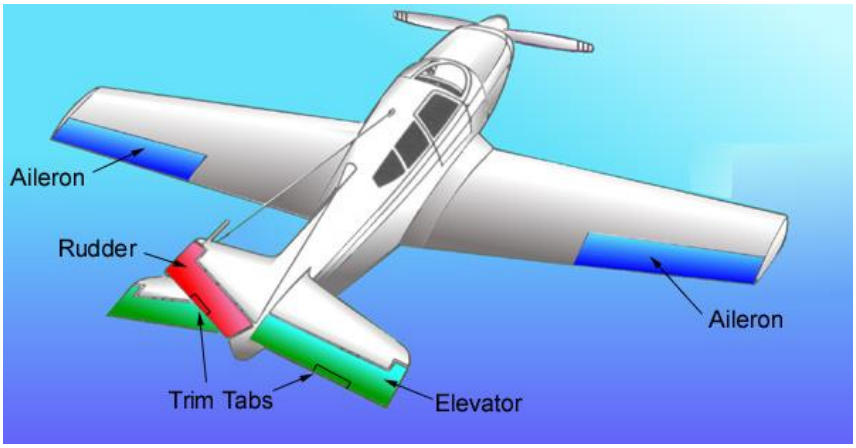

Figure 1.4: placement of main control surfaces of the airplane

1.3.3.2 Secondary controls

There are often secondary controls available to give the pilot finer control over flight or to ease the workload. The most commonly-available control is a wheel or other device to control elevator trim. Most of the aircraft have wing flaps, controlled by a switch or a mechanical lever or in some cases are fully automatic by computer control. Other secondary flight control systems may be available, including slats, spoilers, air brakes and variable-sweep wings.

Figure 1.5: (a) Yoke controller, (b) Center stick controller, (c) Side stick controller

1.3.4 Basic flight control systems

Flight control systems are categorized in to several categories based on the linking mechanism accommodated in between cockpit control devices and control surfaces [10].

1.3.4.1 Mechanical flight control systems

Mechanical flight control systems are the most basic method of controlling an aircraft. They were used in early aircraft and are currently used in small aircraft where the aerodynamic forces are not excessive. A manual flight control system uses a collection of mechanical parts such as rods, tension cables, pulleys, counterweights, and chains. Sometimes forces applied to the cockpit controls transmit directly to the control surfaces. Turnbuckles are often used to adjust control cable tension. -

Increases in control surface area, and higher load generates by high air speed in small air craft, increased the force required to move the control surfaces. Complicated mechanical gearing applications were accommodated to generate large forces from the applied load by pilot.

1.3.4.2 Hydro-mechanical

Mechanical flight control systems became more and more complex and increased weight of the aircraft when aircraft became large in size and grater in performance. Hydro mechanical flight control system was introduced to overcome those limitations caused by the mechanical systems. This has two basic parts. The mechanical circuit consists of rods, cables, pulleys, and sometimes chains which links the cockpit controls with the hydraulic circuits. The hydraulic circuit consists of hydraulic pumps, reservoirs, filters, pipes, valves and actuators. The actuators are powered by the hydraulic pressure generated by the pumps in the hydraulic circuit. The actuators convert hydraulic pressure into control surface movements. To control the movements of the control surfaces the electro-hydraulic servo valves were used.

The pilot's movement of a control causes the mechanical circuit to open the matching servo valve in the hydraulic circuit. The hydraulic circuit powers the actuators which then move the control surfaces. When control surfaces moved to the desired position feedback system gives the signal to close the servo valve to stop the movements of the control surfaces right at the desired position.

With hydro mechanical flight control systems, the load on the surfaces cannot be felt by the pilot. So there is a risk of overstressing the aircraft through excessive control surface movement. To overcome this problem artificial feel systems are used. It consists of mechanism, probably spring mechanism to give the proportional feelings of the generated force on control surfaces.

1.3.4.3 Fly-by-wire control systems

A fly-by-wire system is the latest control system, which replaced manual flight control of an aircraft with an electronic interface. The movements of flight controls are converted to electronic signals are transmitted by wires to the central control computer and control computers determine how to move the actuators at each control surface to provide the expected response. Commands from the computers are also input without the pilot's knowledge to stabilize the aircraft and perform other tasks.

CHAPTER 2

2. Problem Identification

Application of the design and basic requirements of it were discussed in this chapter. Applicable load requirements, functional requirements and testing methods were described in a descriptive manner. Theory behind the testing parameters also described at the end of the chapter.

2.1 Introduction

Side stick control assembly allows pilot to control the roll and pitch of the airplane. Two or more sensors detect the movements of the stick controller and generates correspondence signal. Generated signals are sent to the control computer and computer operates the actuators accordingly. Dual Axis Force Sensor Assembly (DAFSA) is a dual axis force sensor which is going to be employed as a part of the Side stick controller. DAFSA detects the force applied on the side stick by pilot and generates electrical signal proportional to the applied force and send to the control computer of the airplane. Computer controls the pitch and roll of the airplane using the signals. DAFSA basically detects force applied in two orthogonal directions, forward- backward and side to side.

DAFSA is a research and development project conducted in Aerosense Technologies (pvt) ltd to provide development samples for the eligibility testing conducted by the customer. System requirements and space envelop were defined by the customer and mettle foil strain gauge base force transducer was developed to meet the specifications.

2.2 Design specifications

System requirements of the DAFSA were supplied as a document and a source control drawing. Functional requirements and environmental condition requirements were well defined in specification and outer dimensions and the mechanical interfaces of the DAFSA were defined in the source control drawing.

As defined in the specification, DAFSA is a four channel dual axis force sensor. Four channels should be independent, electrically and physically isolated channels. Each independent channel shall consist of a dual axis (Pitch and Roll) force transducer, which are orthogonal to each other. Sensing elements should be connected to the end connectors through wire harnesses.

Applicable load conditions for the DAFSA is defined in the Table 2.1

Table 2.1: Applicable load conditions for the DAFSA

Description	Pitch Axis Force	Roll Axis Force
Normal Operating Load	+/- 60 lbf	+/- 45 lbf
Limit Load	+/- 200 lbf	+/- 100 lbf
Ultimate Load	+/- 300lbf	+/- 150 lbf

Normal operating load is the maximum load that sensors can detect in normal operation.

Limit Load is the maximum amount of force that can be applied without causing any permanent damage to the DAFSA. The DAFSA should continue to meet its normal operating load performance requirements after removal of the limit load.

Ultimate Load is the maximum amount of force that can be applied without losing the structural integrity of the DAFSA. Permanent deformation of the DAFSA is permissible and DAFSA may not continue to meet its normal operating load performance requirements after removal of the ultimate load.

Cross axis forces sensitivity requirements were defined as in Table 2.2. Force sensitivity of each sensor should be less than two present of the applied load when applied load is in perpendicular direction to the measuring direction.

Table 2.2: Cross axis forces sensitivity requirements of DAFSA

Force input direction	Pitch Force Sensor Sensitivity	Roll Force Sensor sensitivity
pitch axis direction	100% lbf	< 2% Pitch force lbf
Roll axis direction	< 2% Roll force lbf	100% lbf

Electrical requirements of DAFSA were defined as follows. Each channel of the DAFSA shall have an excitation voltage of between +/-2.5V to +/-15V and each channel excitation power shall be less than 160mW in parallel across the Pitch and Roll sensors. The output voltage from the sensor shall be a minimum of 0.3mV/lb.

The combination of output sensitivity with the selected excitation voltage shall meet the minimum output voltage requirements as mention above paragraph. The tolerance of the output sensitivity for each channel shall be +/-10%.

Linearity and hysteresis of DAFSA should be within the above mentioned tolerance limit

Weight of the DAFSA shall not exceed 1.35 Lbs. and volume should be as per the source control drawing shown in the appendix A.

Considering electrical requirements DAFSA was designed to have 1mV/V output from each single Wheatstone bridge at full operational load condition.

2.3 Performance testing

DAFSA needed to be tested for compliance against the specifications defined. In this dissertation research only the basic functional requirements of cross axis sensitivity, Linearity, and hysteresis were optimized. Dead load test was performed to evaluate the performance.

DAFSA is a 4 channel dual axis force sensors. Because of that, DAFSA was designed to have 8 force sensors, four force sensors in pitch direction and four in roll direction. Each force sensor consists with 4 strain gauges connected to Wheatstone bridge. Altogether each sensor consists of 32 strain gauges and eight Wheatstone bridges.

2.3.1 Dead load test

In order to evaluate the performance of DAFSA force transducer needed to be tested at known loads in two (pitch and roll) directions. Dead load test rig was designed and fabricated to perform step load tests using dead loads. Figure 2.1 shows the dead load test rig used for testing.

DAFSA was tested in each direction with 15 Lbf ascending load steps up to maximum operating loads and descending load steps back to zero loads. To measure the force sensor output Wheatstone bridge input terminals were excited by one Volt input and measured the voltage output of output terminals. All 8 force sensor outputs were recorded at each and every load steps. Ian Fellows CSW 20 weighing instruments were used for the testing of DAFSA as measuring instrument. Ian Fellows were connected to the Wheatstone bridge and it excites Wheatstone bridge and display the output millivolt value accurate for four decimal places.

Linearity, Hysteresis and cross sensitivity of the sensor were calculated using dead load test results.

Figure 2.1: Dead Load test rig

2.3.2 Parameters of performance

All required test data were gathered using the tasting methods described in section 2.3.1 and analyzed to obtain the performance parameters, namely cross sensitivity percentage, Linearity percentage, and hysteresis percentage of each design.

I. Cross sensitivity percentage

Cross sensitivity percentage value of each channel of the sensor was calculated using following equations.

$$Cross\ sensitivity\ persentage\ value\ of\ pitch\ axis = \frac{P}{Q} \times 100\% \quad (1).$$

$$Cross\ sensitivity\ persentage\ value\ of\ roll\ axis = \frac{R}{S} \times 100\% \quad (2).$$

Where

P – Cross sensitivity of the pitch axis at a load.

Q – Load reading of the roll axis at the same load.

R – Cross sensitivity of the roll axis at a load.

S – Load reading of the pitch axis at the same load.

II. Nonlinearity

Non linearity of the sensor defined as fallows and calculations were based on the Figure 2.2.

$$Non\ Linearity = \left(\frac{V_a - V_o}{V_o}\right) \times 100\% \quad (3).$$

$$V_o = \frac{V_f}{L_f} \times L_o \quad (4).$$

By substituting (4) in (3)

$$Non\ Linearity = \left(\frac{V_a - \left(\frac{V_f}{L_f} \times L_o\right)}{\frac{V_f}{L_f} \times L_o}\right) \times 100\% \quad (5).$$

$$Non\ Linearity = \left(\frac{V_a L_f - V_f L_o}{V_f L_o}\right) \times 100\% \quad (6).$$

Where

V_a - Output reading at load L_o.

L_f – Normal operating load (Full load).

V_f - Output reading at full load.

III. Hysteresis

Hysteresis calculation is based on Figure 2.2 and shows below.

$$Hysteresis = \left(\frac{V_a - V_d}{V_o}\right) \times 100\% \quad (7).$$

Substituting (4) in (7)

$$Hysteresis = \left(\frac{V_a - V_d}{\frac{V_f}{L_f} \times L_o}\right) \times 100\% \quad (8).$$

$$Hysteresis = \left(\frac{V_a - V_d}{V_f}\right) \times \frac{L_f}{L_o} \times 100\% \quad (9).$$

Where

V_d - output reading at load L_o at descending loads.

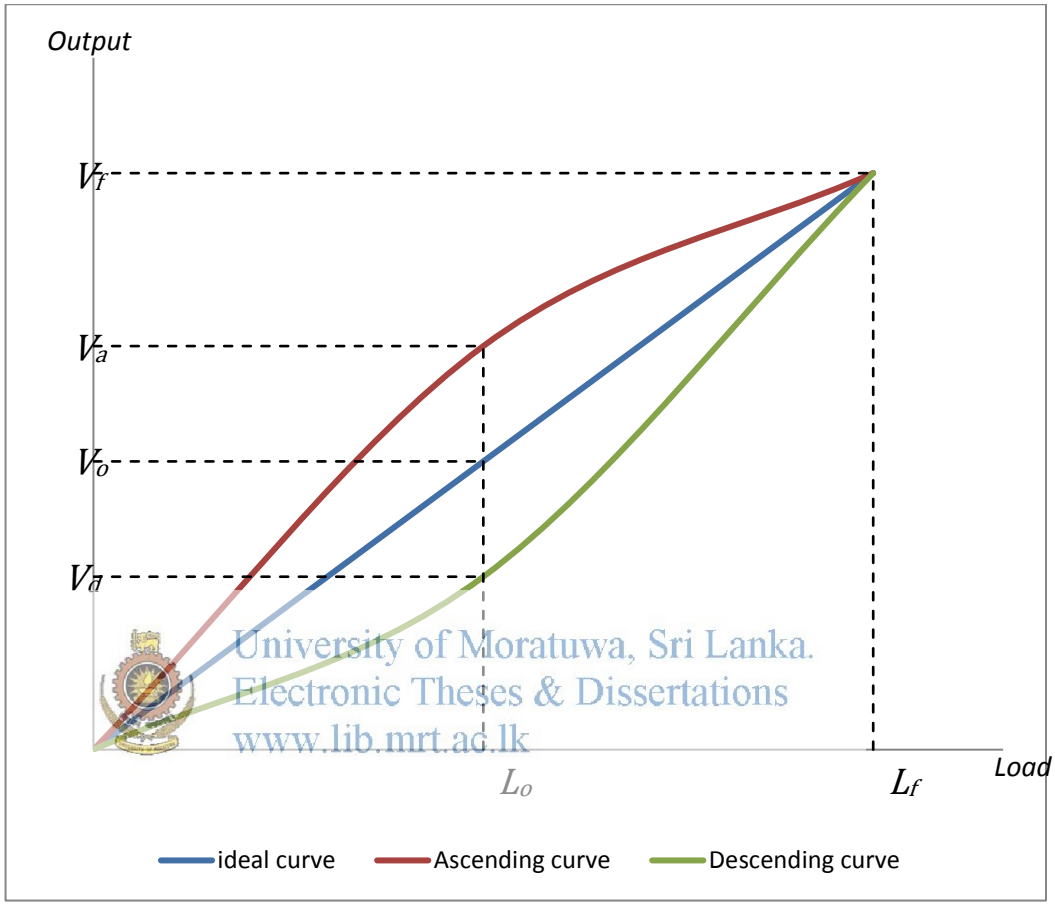

Figure 2.2: Real output curves and ideal output curve against load

3. Preliminary Design Concept

This chapter described about the first three preliminary design concepts. Design stage concerns and design out comes are described briefly. Fabrication method of the first three models, practical issues occurred during fabrication and testing are discussed. Test results and the analysis are also included.

3.1 Conceptual Designs

Preliminary stage of the project was directed towards the searching of suitable structural design for the DAFSA. At very first stage of the design three conceptual models were developed. Conventional load cell models structures were not suitable for dual axis requirement. Innovative three ideas of structural designs were develop into the Solid Works 3D models.

3.1.1 Material Selection

At the beginning of the design it was needed to be decided two major materials for modeling and fabrications of sensors.

1. Metal for structural fabrication

Aluminum alloy AL2024-T4 was selected as element material. Yield strength, young's modules and ultimate tensile strength of material was matched with system requirements. In addition to the material properties size of the strain gage was also considered as a factor for material selection. Cost of material and machining also played major roll in material selection process.

2. Strain gauge

For preliminary testing "strain gage 0.062x0.062; 350 OHM" strain gage selected due to low cost, better lead time and the availability. It was manufactured by Flintec (Pvt) Ltd, Sri Lanka.

3.1.2 Three structural Designs

Three conceptual models were designed using Finite Element Analysis in Solid Works. They were named as Concept 1, Concept 2, and Concept 3.

3D model of the concept 1 design is shown in Figure 3.1 and it consists of four straight columns with filet ends. Strain gauges were pasted on all four columns. Each column has eight strain gauges bonded, two strain gauges per each side top and

bottom of the column. Figure 3.2 shows the strain gauge placement of the concept 1, and yellow color elements are the strain gauges. Each column was considered as one dual axis force sensor. Two strain gauges pasted on one side and other two of the opposite side of same column were connected in to one Wheatstone bridge and it was considered as the one direction force sensor. Remaining four strain gauges were connected to separate Wheatstone bridge and considered as force sensor in other direction.

According to the design each Wheatstone bridge output should be one millivolt per one volt input at the full load condition. To full fill the above requirement, mean strain value of the area under grid area of strain gauge should be 500 micro strains at full load condition. Using solid works Finite Element Analysis (FEA) beam thickness, width and length were adjusted to match with the strain requirements.

Figure 3.1: Concept 1 solid model

Figure 3.2: Strain gauge placement on single column.

Concept 2 has few similarities to the concept 1. But concept 2 space envelop is different from the concept 1. Concept 2 contains additional four columns than concept 1, totally it contains with eight columns. Figure 3.3 is solid model of concept 2.

Strain gauges were pasted on four columns as same manner in concept 1. Four columns placed in four corners were selected to paste strain gauges. Other four columns were placed as load distributers.

One column of the sensor was also considered as one dual axis force sensor and wire connection was as same as concept 1.

Figure 3.3: Concept 2 solid model

Concept 3 is deferent from first two concepts and it consists four separate columns in two stages. Figure 3.4 illustrates third conceptual design. Wire connection was as same as first two.

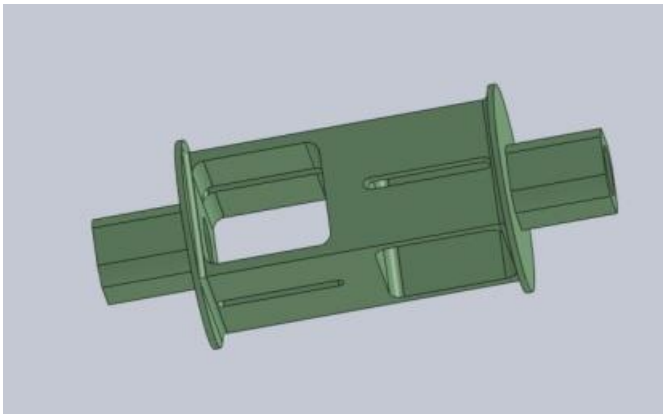

Figure 3.4: Concept 3 solid model

3.2 Fabrications

Three design models were converted in to the machine drawings with appropriate tolerances. Metal parts were machined by outsources party using precise CNC machineries and delivered to the factory with grate safe. Incoming inspections were performed as per the drawing which highlighting all critical dimensions. Incoming inspection passed metal parts were handed over for the cleaning process. After finished the degreasing process it was ready to the most important and critical process in strain gauge base force sensor industry called gauging.

Gauging process means basically a strain gauge bonding process on the metal sensor bodies. This was performed in two major steps called bonding and curing.

Strain gauge position is most critical parameter which effect to the desired performance of the force sensor. Therefore designed relative positions of the strain gauges were supplied with a drawing to operator and he performed the making position marks on the metal. Gauge blocks which have precisely machined flat parallel surfaces and digital height gauge were used during the process as required. Figure 3.5 shows the usage of instrument during gauge position making process.

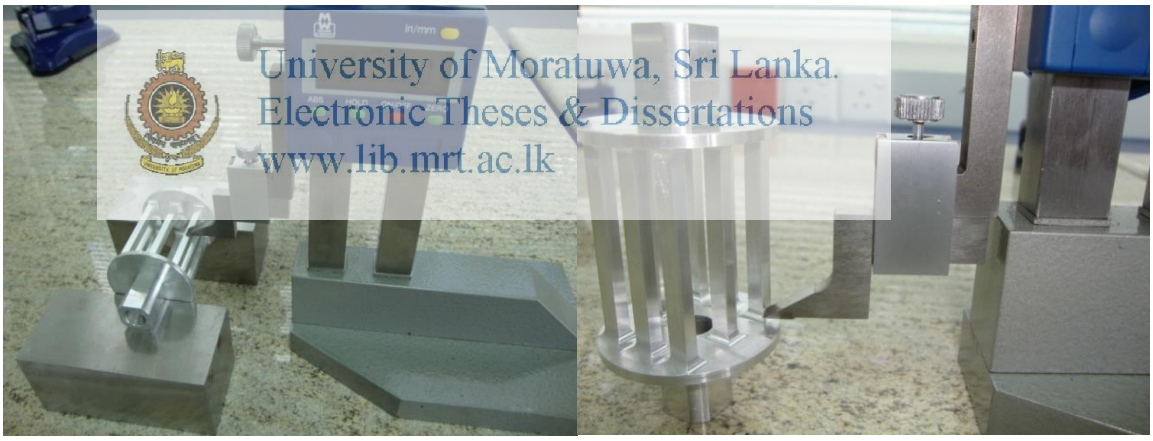

Figure 3.5: Strain gauge position marking process

Next step was inspection and preparation for bonding of strain gauges. Each and every strain gauge was carefully inspected for manufacturing defect before performing any operation in order to prevent reworks. Thereafter all the required number of strain gauges were laid on glass plate and stick a strip of tape on top of the strain gauge and were positioned as shown in the Figure 3.6 for apply bonding agent. Then bonding agent was applied evenly on each strain gauge and metal body and kept in room condition around half an hour time till set the bonding agent.

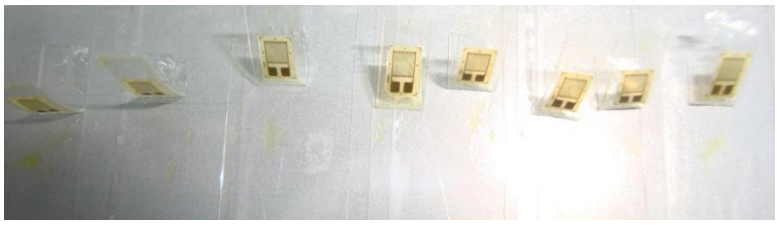

Figure 3.6: Strain gauge prepared for apply bonding adhesive

Once bonding agent set it is possible to recognize visually with an experience. Pasting strain gauges on correct position was performed by the experienced operator with use of microscope. Total process above described was performed under clean room condition to prevent mitigation of contaminant between the strain gauge and metal surface.

Bonded strain gauges should cure in an oven for three hours in temperature 160 ℃ and need to cool in oven. Furthermore it is necessary to maintain 50 Lbf/in^2 pressure on the strain gauge during the curing cycle in order to have proper bonding. Figure 3.7 shows the mechanism that made out using springs and thread bars to pressure the strain gauges. Silicon pads were used in between strain gauges and pressure palate in order to maintain even distribution of pressure and prevent the damaging the strain gauges. After finish the curing cycle it is required to remove tapes, clean and proper inspection. According to the designs of first three models of sensors were required to have 2 to 6 cycles of bonding in order to finish the bonding of the one sensor. Concept 1 required to have 6 cycles of bonding, concept 2 required to have 4 cycles and concept 3 required to have only 2 cycles of bonding.

Figure 3.7: Bonding clamp mechanism

Once it was confirmed all the strain gauges were bonded properly and no damage of strain gauges they were moved to wiring process.

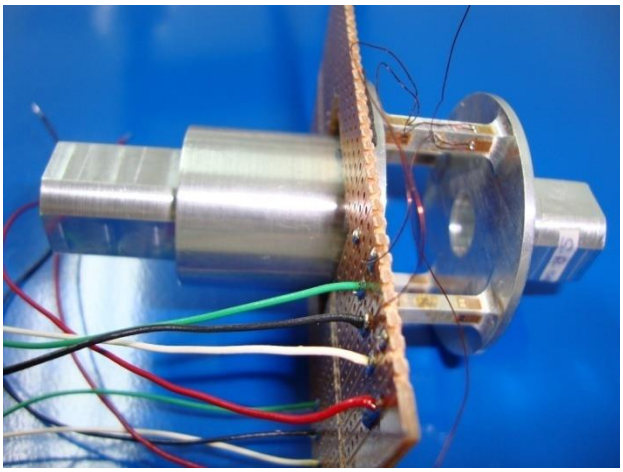

Figure 3.8: Example of sensor wiring

As shown in the Figure 3.8 wires started from the strain gauges were routed to the circuit board and from the circuit board, four wires were extended for testing purposes. To wires to excitation of the Wheatstone bridge and other two is for measure the output of Wheatstone bridge.

3.3 Practical issues

During the fabrication of the sensors, lots of practical problems were occurred. Most of the cases were occurred during the bonding process. Figure 3.9 (a) shows one damaged strain gauge during the removal process of the tape after curing cycle. This was happened due to the in proper bonding of the strain gauge. According to the analysis results strain gauges were placed very closer to the columns end and small portion of the gauges were bonded over the curved surface also. Each and every cases we had experienced the strain gauges were damaged from the side which pasted on the curved surface. That side of the strain gauges was not bonded properly.

As required per the design, all sensing elements were under gone in more than one cycles of curing in oven. It was experienced after second cycle of the curing first bonded set of strain gauges were colour changed.

After finished the bonding of the elements, wring process was started with 34 AWG gauge insulated wires and directly soldered to the solder tab of the strain gauges. While doing the wiring few tabs of the strain gauges were came off with the wire because of the high stiffness of the wire. Figure 3.9 (b) shows an example.

Most of the Wheatstone bridges were not balanced at the zero loads. It showed some significant zero unbalance and it badly effect during the testing. Because of the initial

shift, Wheatstone bridges output values were beyond the measuring range of the measuring instrument and they were unable to test at higher loads.

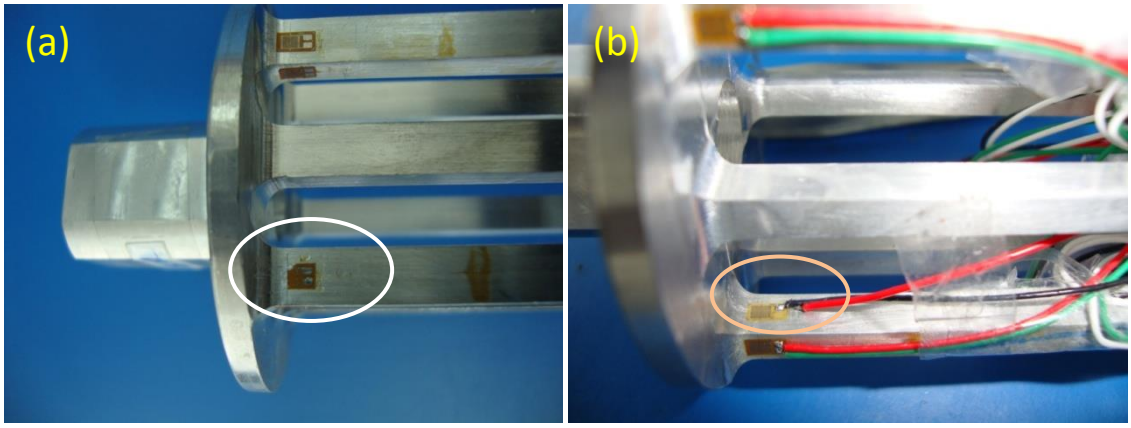

Figure 3.9: Examples of Damaged strain gauges during fabrications

3.4 Tests and test results

As described in the section 2.3 tests were conducted for each and every conceptual model. Following tables contains those test results. P1, P2, P3 and P4 are four channels (Wheatstone bridges) in pitch direction and R1, R2, R3, and R4 are channels (Wheatstone bridges) in roll direction. Table 3.1 and Table 3.2 shows the dead load test results of concept 1 in pitch and roll directions respectively. Table 3.3 and Table 3.4 contain the dead load test results of concept 2 in pitch and roll directions respectively. Same way, content of the Table 3.5 and Table 3.6 are dead load test results of concept 3 in pitch and roll directions respectively. Concept 2 and concept 3 sensors had some defected channels as mention in section 3.3, those were not tested and remain blank in test result tables.

Table 3.1: Load test results of Concept 1, Pitch direction

Load (lbf)	Output (mV/V) Bridge No.							
	P1	P2	P3	P4	R1	R2	R3	R4
00			0.0000			0.0000		0.0000
15			-0.0914			0.0233		-0.0339
30			-0.2154			0.0464		-0.0674
45			-1.3448			-0.0259		0.0120
60			-2.4925			-0.1007		0.0935
45			-1.3436			-0.0264		0.0121
30			-0.2214			0.0465		-0.0667
15			-0.0896			0.0239		-0.0338
00			0.0000			0.0000		-0.0001

Table 3.2: Load test results of concept 1, Roll direction

Load (lbf)	Output (mV/V) Bridge No.							
	P1	P2	P3	P4	R1	R2	R3	R4
00			0.0000			0.0000		0.0000
15			-0.0041			-0.1851		-0.1711
30			-0.0067			-0.3738		-0.3429
45			-0.0083			-0.5648		-0.5154
30			-0.0065			-0.3718		-0.3418
15			-0.0039			-0.1836		-0.1707
00			0.0000			0.0001		-0.0004

Table 3.3: Load test results of Concept 2, Pitch direction

Load (lbf)	Output (mV/V) Bridge No.							
	P1	P2	P3	P4	R1	R2	R3	R4
00	0.0000	0.0000	0.0000	0.0000		0.0000		
15	-0.2945	-0.2618	-0.2777	0.2765		0.0744		
30	-0.5875	-0.5417	-0.5514	0.5540		0.1532		
45	-0.8832	-0.8125	-0.8287	0.8236		0.2245		
60	-1.1740	-1.0846	-1.1056	1.1095		0.2928		
45	-0.8735	-0.8142	-0.8306	0.8364		0.2223		
30	-0.5885	-0.5398	-0.5510	0.5523		0.1475		
15	-0.2930	-0.2652	-0.2761	0.2740		0.0729		
00	0.0000	0.0054	0.0024	0.0000		-0.0003		

Table 3.4: Load test results of concept 2, Roll direction

Load (lbf)	Output (mV/V) Bridge No.							
	P1	P2	P3	P4	R1	R2	R3	R4
00	0.0000	0.0000	0.0003	0.0000		0.0000		
15	0.0709	-0.0411	0.0514	0.0679		-0.3573		
30	0.1410	-0.0812	0.1038	0.1357		-0.7132		
45	0.2120	-0.1258	0.1569	0.1982		-1.0708		
30	0.1421	-0.0827	0.1062	0.1309		-0.7113		
15	0.0717	-0.0392	0.0507	0.0672		-0.3540		
00	0.0001	0.0017	-0.0008	0.0000		0.0028		

Table 3.5: Load test results of Concept 3, Pitch direction

Load (lbf)	Output (mV/V) Bridge No.							
	P1	P2	P3	P4	R1	R2	R3	R4
00	0.0000	0.0000	0.0000	0.0000	0.0000		0.0000	
15	-0.3221	-0.3187	0.3045	0.3080	-0.0440		-0.0475	
30	-0.6445	-0.6374	0.6166	0.6163	-0.0960		-0.0983	
45	-0.9673	-0.9569	0.9161	0.9230	-0.1435		-0.1480	
60	-1.2901	-1.2760	1.2185	1.2301	-0.1930		-0.1975	
45	-0.9681	-0.9563	0.9119	0.9206	-0.1430		-0.1486	
30	-0.6464	-0.6371	0.6079	0.6150	-0.0965		-0.0984	
15	-0.3233	-0.3183	0.3026	0.3052	-0.0485		-0.0493	
00	0.0000	0.0002	0.0003	0.0000	-0.0002		-0.0001	

Table 3.6: Load test results of concept 3, Roll direction

Load (lbf)	Output (mV/V) Bridge No.							
	P1	P2	P3	P4	R1	R2	R3	R4
00	0.0000	0.0000	0.0000	0.0000	0.0000		0.0000	
15	0.2261	-0.2324	-0.2341	0.2259	-0.4243		-0.4256	
30	0.4518	-0.4640	-0.4656	0.4515	-0.8469		-0.8513	
45	0.6765	-0.6955	-0.6976	0.6757	-1.2708		-1.2745	
30	0.4534	-0.4640	-0.4631	0.4526	-0.8467		-0.8495	
15	0.2275	-0.2307	-0.2311	0.2274	-0.4237		-0.4242	
00	-0.0002	0.0001	0.0007	0.0001	0.0001		0.0009	

3.5 Test results analysis

As described in section 2.3.2 percentage cross sensitivity value, nonlinearity and hysteresis values were calculated for each channel (Wheatstone bridge) and resultants are shown below. Values of each table were drawn in a graph below each table.

Table 3.7: Percentage cross sensitivity values of pitch axis, concept 1

Load (lbf)	percentage value of concept 1pitch axis cross sensitivity%			
Ascending	P1	P2	P3	P4
0			0.00%	
15			2.40%	
30			1.95%	
45			1.61%	
Descending				
45			1.61%	
30			1.90%	
15			2.28%	
0			0.00%	

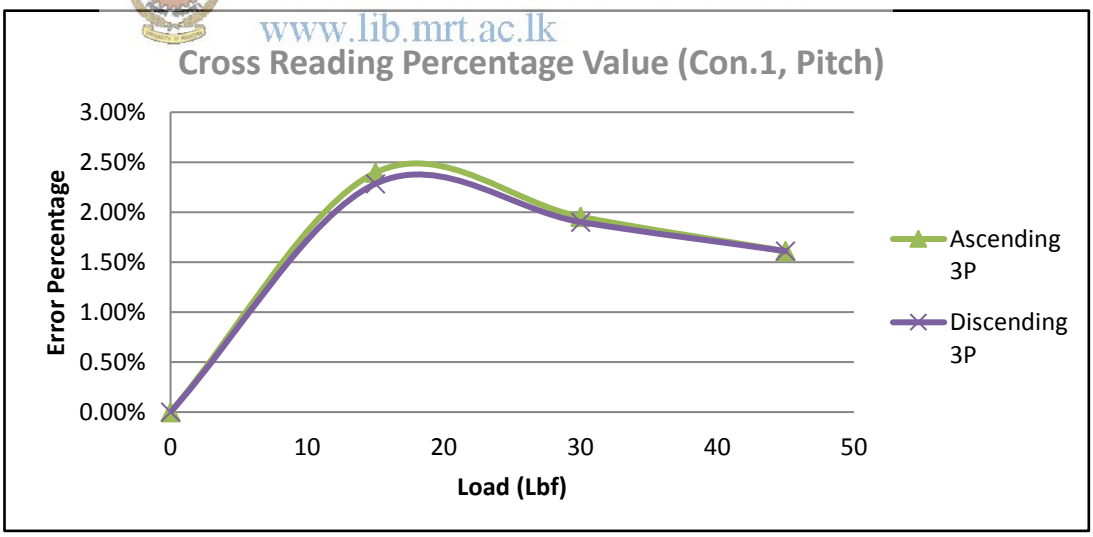

Figure 3.10: Percentage cross sensitivity graph of pitch axis, concept 1

Table 3.8: Percentage non linearity values of pitch axis, concept 1

Load (lbf)	Percentage value of concept 1 pitch axis Non linearity %			
Ascending	P1	P2	P3	P4
0			0.00%	
15			-21.33%	
30			-41.36%	
45			-21.05%	
60			0.00%	
Descending				
60			0.00%	
45			-21.09%	
30			-41.12%	
15			-21.41%	
0			0.00%	

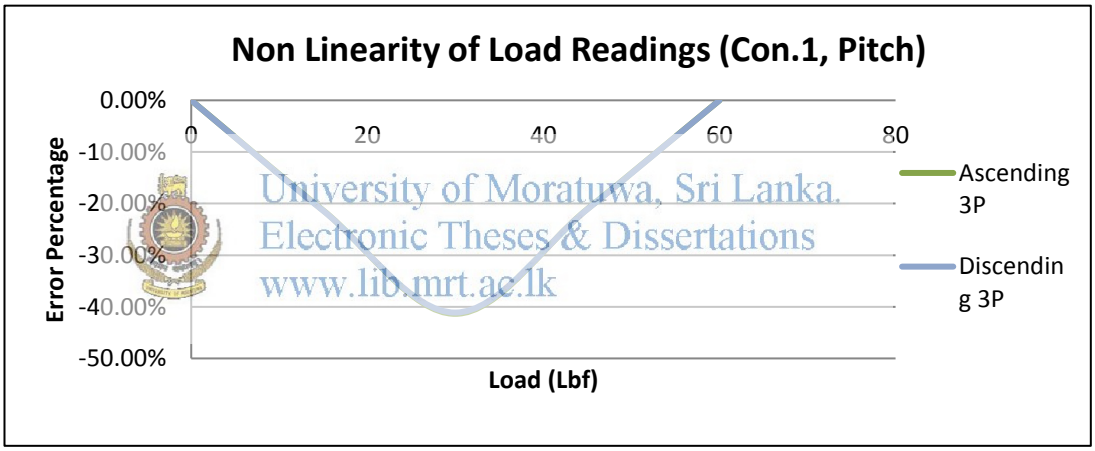

Figure 3.11: Percentage non linearity graph of pitch axis, concept 1

Table 3.9: Percentage hysteresis values of pitch axis, concept 1

Load (lbf)	Percentage value of concept 1pitch axis Hysteresis %			
	P1	P2	P3	P4
0			0.00%	
15			-0.07%	
30			0.24%	
45			-0.05%	
60			0.00%	

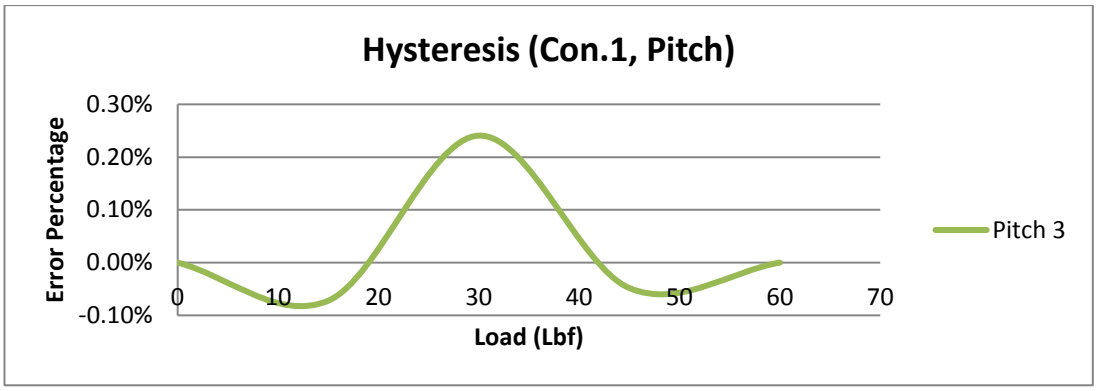

Figure 3.12: Percentage hysteresis graph of pitch axis, concept 1

Table 3.10: Percentage cross sensitivity values of roll axis, concept 1

Load (lbf)	percentage value of concept 1roll axis cross sensitivity%			
Ascending	1R	2R	3R	4R
0		0.00%		0.00%
15		-25.49%		37.09%
30		-21.54%		31.29%
45		1.93%		-0.89%
60		4.04%		-3.75%
Descending				
60		4.04%		-3.75%
45		1.96%		-0.90%
30		-21.00%		30.13%
15		-26.67%		37.72%
0		0.00%		0.00%

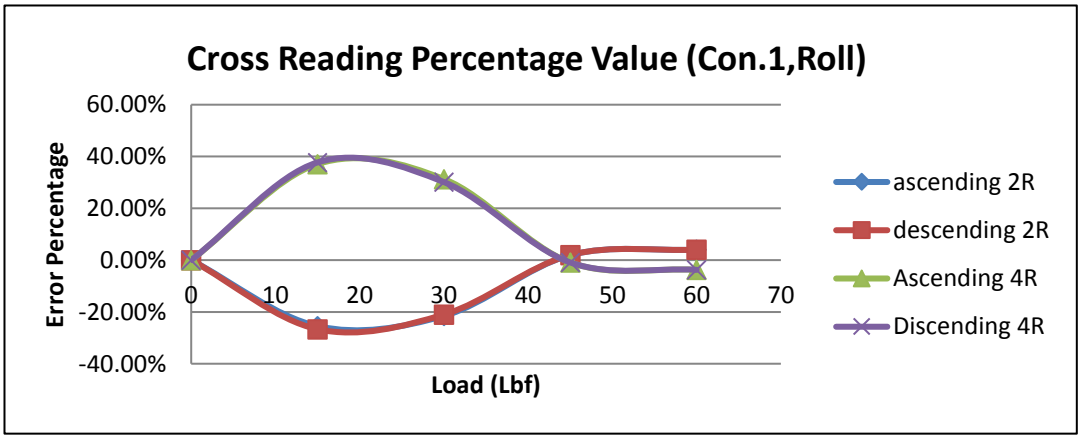

Figure 3.13: Percentage cross sensitivity graph of roll axis, concept 1

Table 3.11: Percentage non linearity values of roll axis, concept 1

Load (lbf)	Percentage value of concept 1 roll axis non linearity %			
Ascending	1R	2R	3R	4R
0		0.00%		0.00%
15		-0.56%		-0.14%
30		-0.48%		-0.14%
45		0.00%		0.00%
Descending				
45		0.00%		0.00%
30		-0.84%		-0.35%
15		-0.83%		-0.21%
0		-0.02%		0.08%

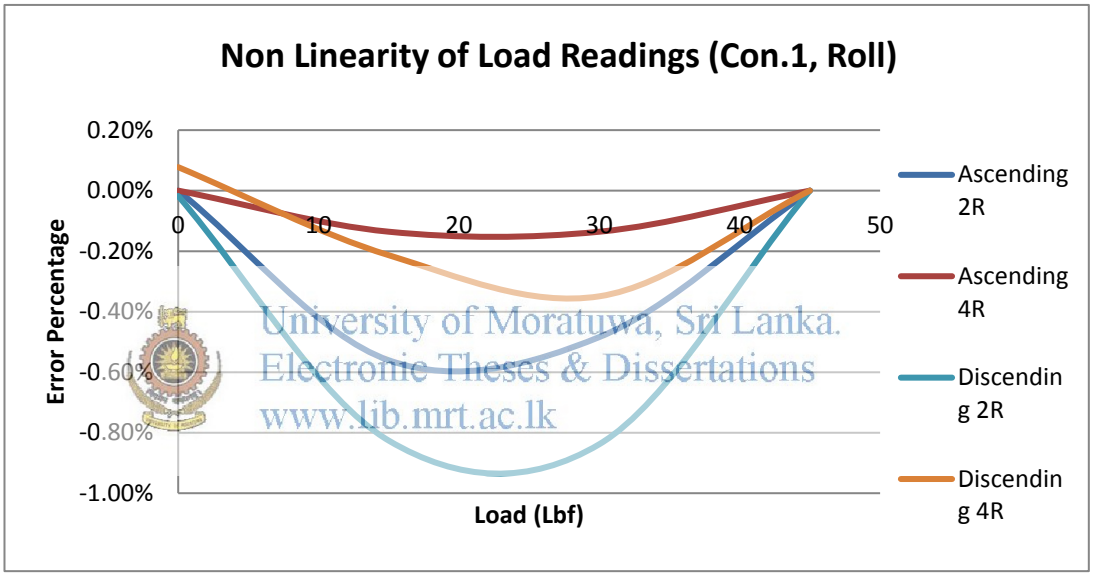

Figure 3.14: Percentage non linearity graph of roll axis, concept 1

Table 3.12: Percentage hysteresis values of roll axis, concept 1

Load (lbf)	Percentage value of concept 1roll axis hysteresis %			
	1R	2R	3R	4R
0		-0.02%		0.08%
15		-0.27%		-0.08%
30		-0.35%		-0.21%
45		0.00%		0.00%

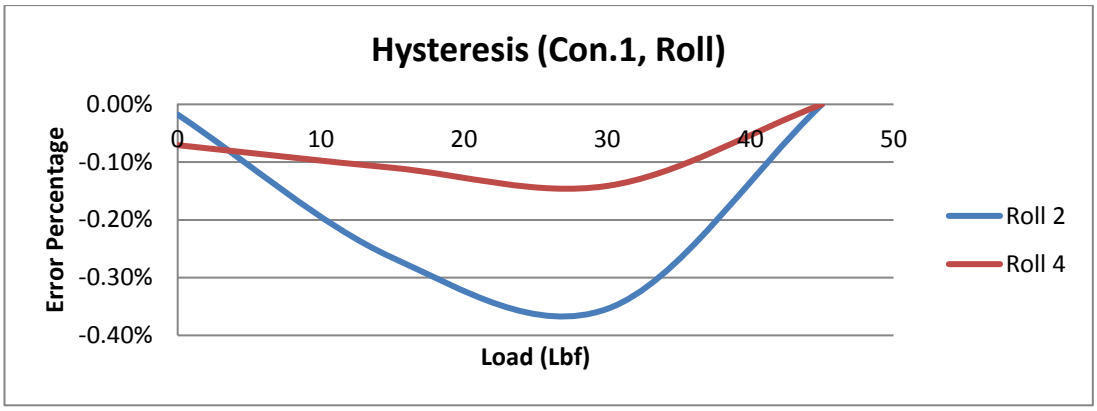

Figure 3.15: Percentage hysteresis graph of roll axis, concept 1

Table 3.13: Percentage cross sensitivity values of pitch axis, concept 2

Load (lbf)	percentage value of concept 2 pitch axis cross sensitivity%			
Ascending	1P	2P	3P	4P
0	0.00%	0.00%	0.00%	0.00%
15	-19.84%	11.50%	-14.39%	-19.00%
30	-19.77%	11.39%	-14.55%	-19.03%
45	-19.80%	11.75%	-14.65%	-18.51%
Descending				
45	-19.80%	11.75%	-14.65%	-18.51%
30	-19.98%	11.63%	-14.93%	-18.40%
15	-20.25%	11.07%	-14.32%	-18.98%
0	0.00%	0.00%	0.00%	0.00%

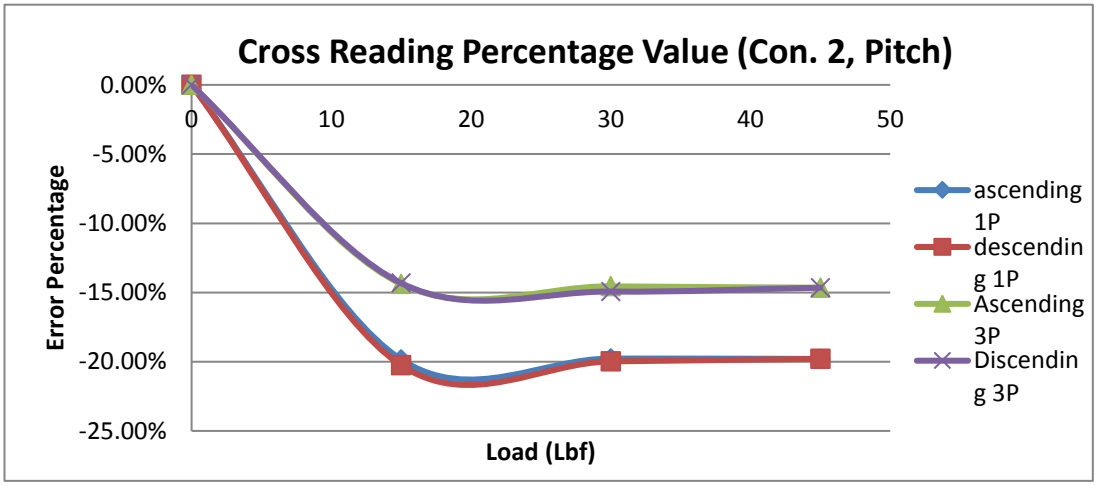

Figure 3.16: Percentage cross sensitivity graph of pitch axis, concept 2

Table 3.14: Percentage non linearity values of pitch axis, concept 2

Load (lbf)	percentage value of concept 2 pitch axis non linearity %			
Ascending	1P	2P	3P	4P
0	0.00%	0.00%	0.00%	0.00%
15	0.09%	-0.86%	0.12%	-0.08%
30	0.04%	-0.06%	-0.13%	-0.07%
45	0.23%	-0.09%	-0.05%	-0.77%
60	0.00%	0.00%	0.00%	0.00%
Descending				
60	0.00%	0.00%	0.00%	0.00%
45	-0.60%	0.07%	0.13%	0.39%
30	0.13%	-0.23%	-0.16%	-0.22%
15	-0.04%	-0.55%	-0.03%	-0.30%
0	0.00%	-0.50%	-0.22%	0.00%

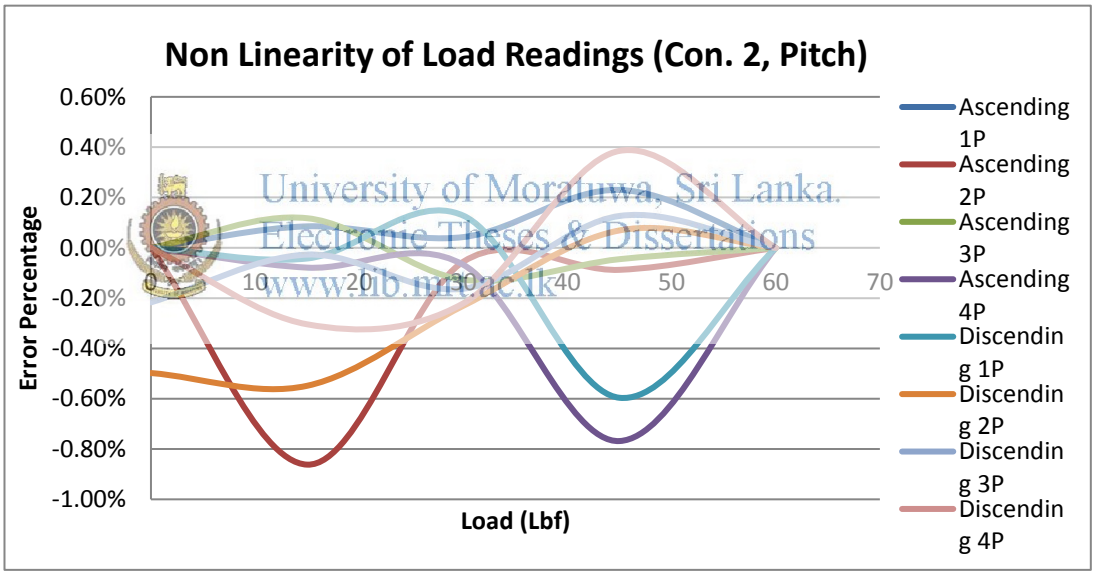

Figure 3.17: Percentage non linearity graph of pitch axis, concept 2

Table 3.15: Percentage hysteresis values of pitch axis, concept 2

Load (lbf)	percentage value of concept 2 pitch axis hysteresis %			
	1P	2P	3P	4P
0	0.00%	-0.50%	-0.22%	0.00%
15	-0.13%	0.31%	-0.14%	-0.23%
30	0.09%	-0.18%	-0.04%	-0.15%
45	-0.83%	0.16%	0.17%	1.15%
60	0.00%	0.00%	0.00%	0.00%

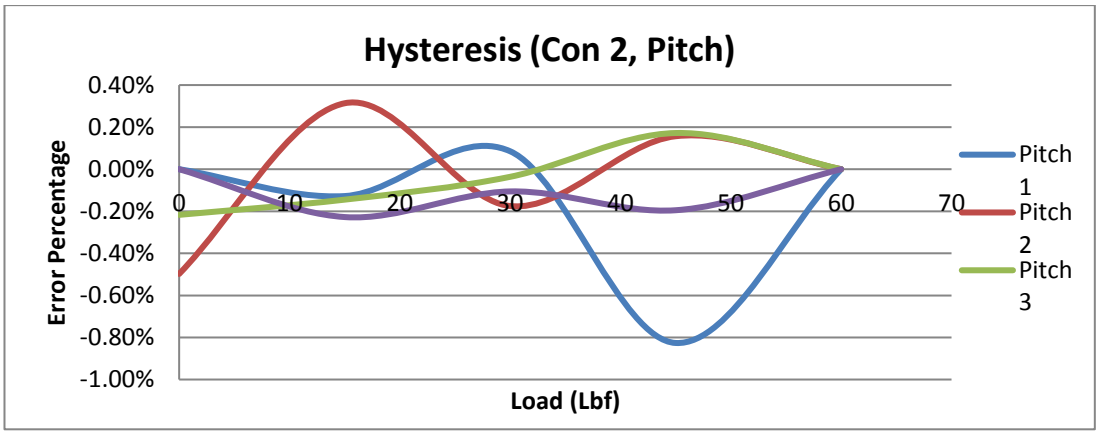

Figure 3.18: Percentage hysteresis values of pitch axis, concept 2

Table 3.16: Percentage cross sensitivity values of roll axis, concept 2

Load (lbf)	percentage value of concept 2 roll axis cross sensitivity%			
Ascending	1R	2R	3R	4R
0		0.00%		
15		-26.79%		
30		-27.78%		
45		-27.09%		
60		-26.48%		
Descending				
60		-26.48%		
45		-26.76%		
30		-27.77%		
15		-26.40%		
0		0.00%		

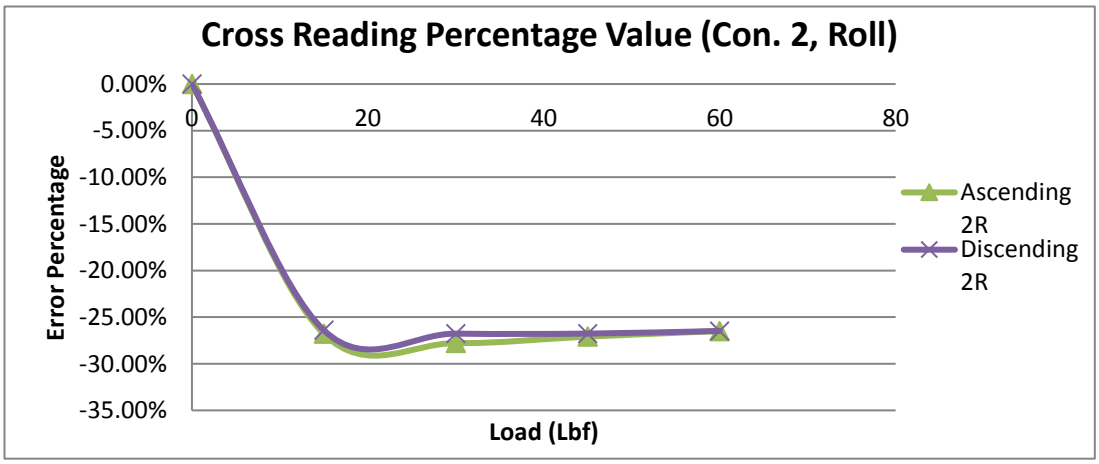

Figure 3.19: Percentage cross sensitivity graph of roll axis, concept 2

Table 3.17: Percentage non linearity values of roll axis, concept 2

Load (lbf)	percentage value of concept 2 roll axis Non linearity %			
Ascending	1R	2R	3R	4R
0		0.00%		
15		0.03%		
30		-0.06%		
45		0.00%		
Descending				
45		0.00%		
30		-0.24%		
15		-0.27%		
0		-0.26%		

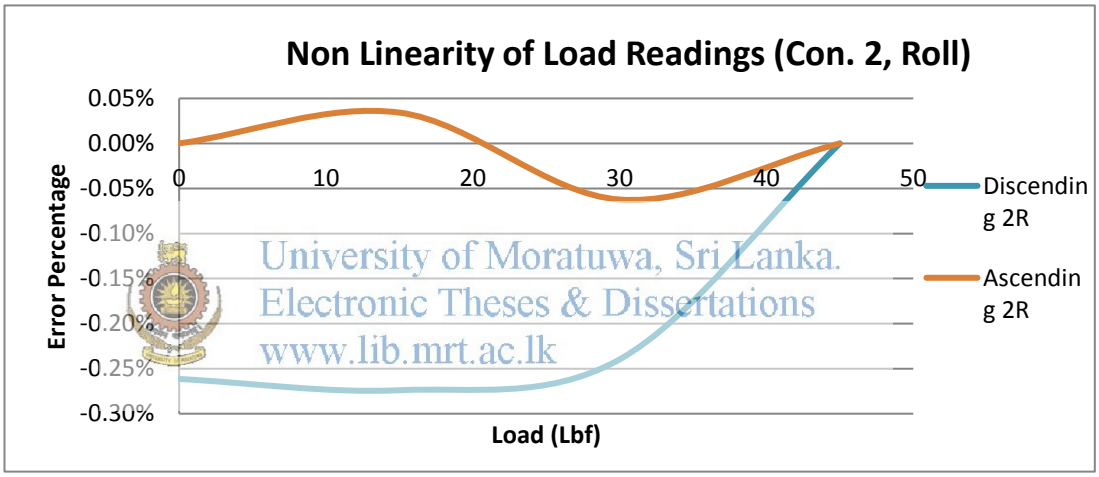

Figure 3.20: Percentage non linearity graph of roll axis, concept 2

Table 3.18: Percentage hysteresis values of roll axis, concept 2

Load (lbf)	percentage value of concept 2 roll axis Hysteresis %			
	1R	2R	3R	4R
0		-0.26%		
15		-0.31%		
30		-0.18%		
45		0.00%		

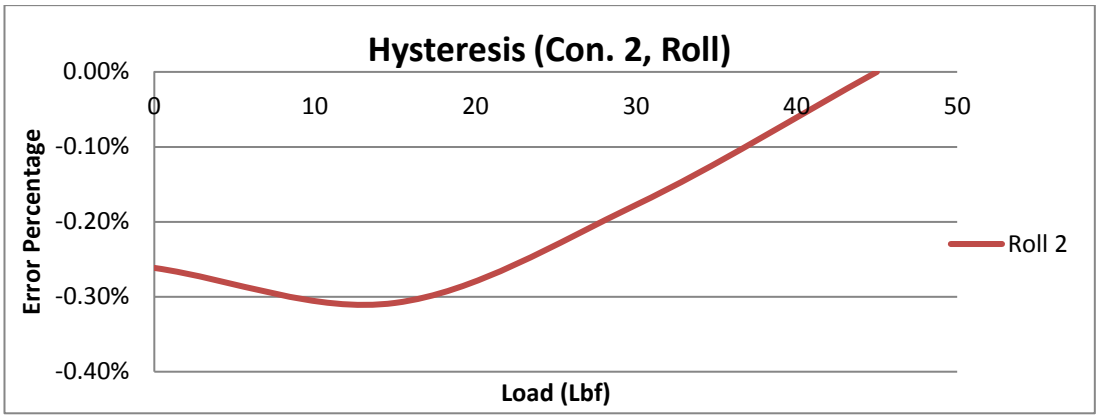

Figure 3.21: Percentage hysteresis graph of roll axis, concept 2

Table 3.19: Percentage cross sensitivity values of pitch axis, concept 3

Load (lbf)	percentage of cross sensitivity%			
Ascending	P1	P2	P3	P4
0	0.00%		0.00%	
15	-53.29%		55.00%	
30	-53.35%		54.69%	
45	-53.23%		54.74%	
Descending				
45	-53.23%		54.74%	
30	-53.55%		54.51%	
15	-53.69%		54.48%	
0	0.00%		0.00%	

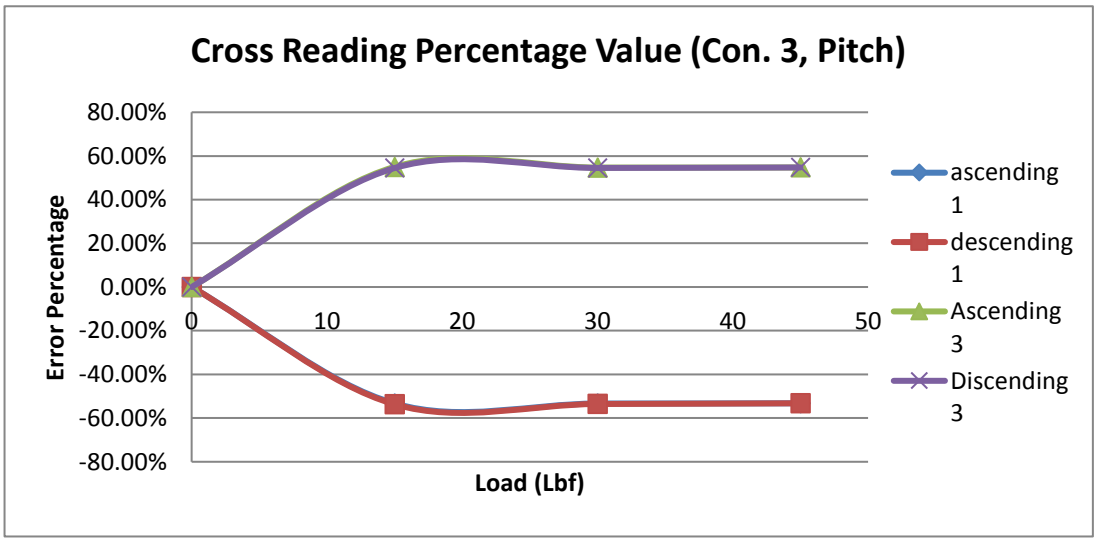

Figure 3.22: Percentage cross sensitivity graph of pitch axis, concept 3

Table 3.20: Percentage non linearity values of pitch axis, concept 3

Load (lbf)	Non linearity %			
Ascending	P1	P2	P3	P4
0	0.00%	0.00%	0.00%	0.00%
15	-0.03%	-0.02%	-0.01%	0.04%
30	-0.04%	-0.05%	0.60%	0.10%
45	-0.02%	-0.01%	0.18%	0.03%
60	0.00%	0.00%	0.00%	0.00%
Descending				
60	0.00%	0.00%	0.00%	0.00%
45	0.04%	-0.05%	-0.16%	-0.16%
30	0.10%	-0.07%	-0.11%	0.00%
15	0.06%	-0.05%	-0.17%	-0.19%
0	0.00%	-0.02%	0.02%	0.00%

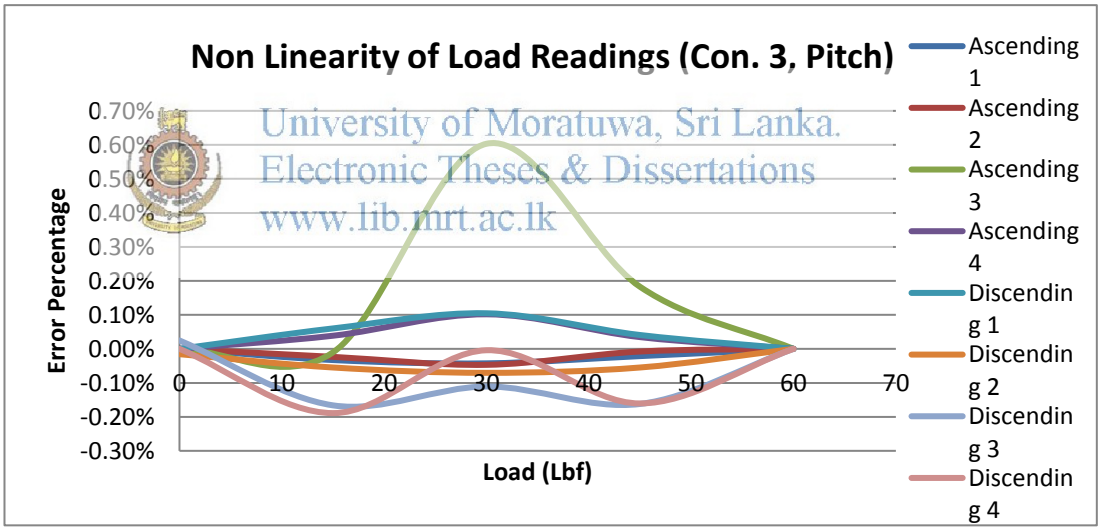

Figure 3.23: Percentage non linearity graph of pitch axis, concept 3

Table 3.21: Percentage hysteresis values of pitch axis, concept 3

Load (lbf)	Hysteresis %			
	P1	P2	P3	P4
0	0.00%	-0.02%	0.02%	0.00%
15	0.09%	-0.03%	-0.16%	-0.23%
30	0.15%	-0.02%	-0.71%	-0.11%
45	0.06%	-0.05%	-0.34%	-0.20%
60	0.00%	0.00%	0.00%	0.00%

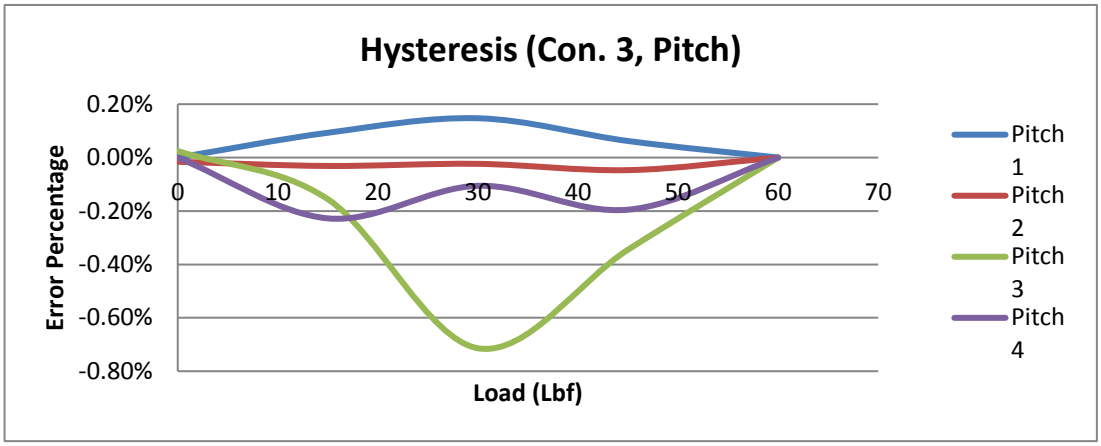

Figure 3.24: Percentage hysteresis graph of pitch axis, concept 3

Table 3.22: Percentage cross sensitivity values of roll axis, concept 3

Load (lbf)	percentage of cross sensitivity%			
Ascending	R1	R2	R3	R4
0	0.00%		0.00%	
15	13.66%		-15.60%	
30	14.90%		-15.94%	
45	14.84%		-16.16%	
60	14.96%		-16.21%	
Descending				
60	14.96%		-16.21%	
45	14.77%		-16.30%	
30	14.93%		-16.19%	
15	15.00%		-16.29%	
0	0.00%		0.00%	

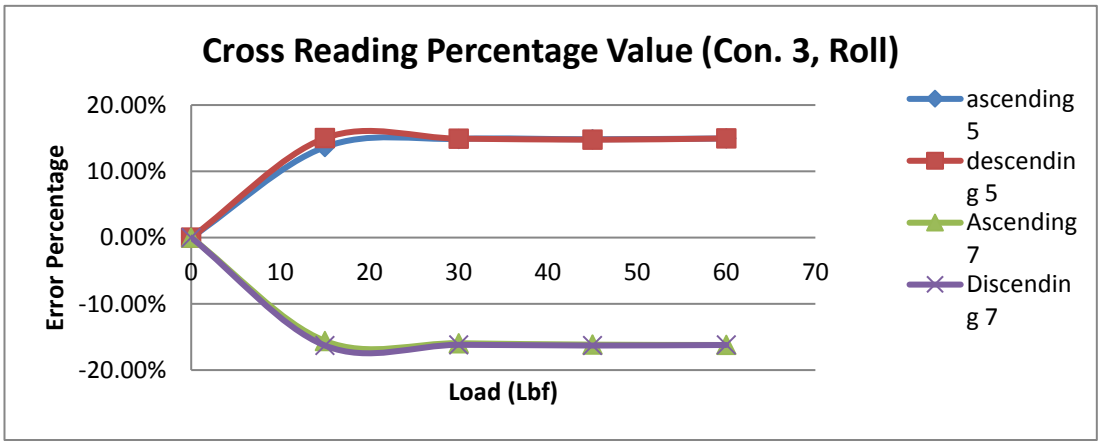

Figure 3.25: Percentage cross sensitivity graph of roll axis, concept 3

Table 3.23: Percentage non linearity values of roll axis, concept 3

Load (lbf)	Non linearity %			
Ascending	R1	R2	R3	R4
0	0.00%		0.00%	
15	0.06%		0.06%	
30	-0.02%		0.13%	
45	0.00%		0.00%	
Descending				
45	0.00%		0.00%	
30	-0.04%		-0.01%	
15	0.01%		-0.05%	
0	-0.01%		-0.07%	

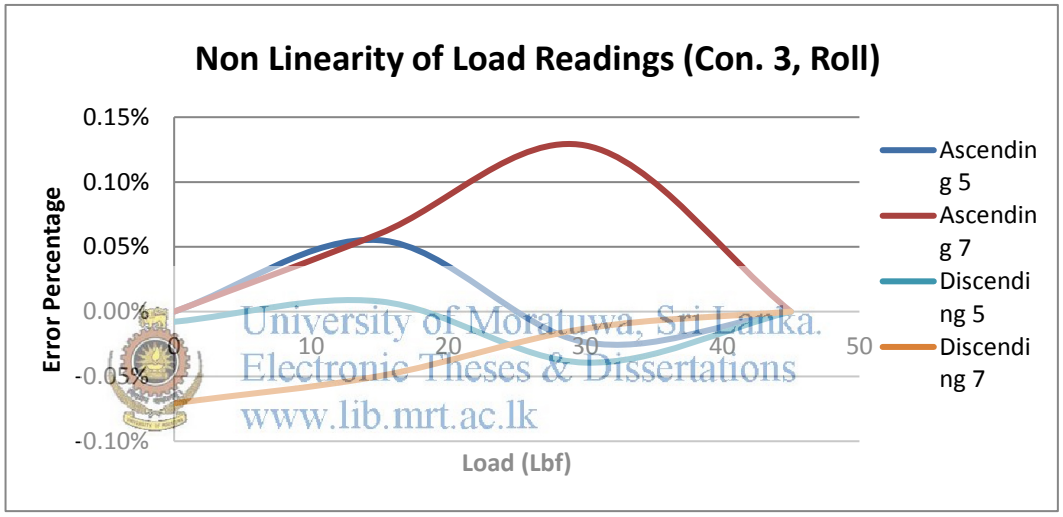

Figure 3.26: Percentage non linearity graph of roll axis, concept 3

Table 3.24: Percentage hysteresis values of roll axis, concept 3

	Hysteresis %			
Load (lbf)	R1	R2	R3	R4
0	-0.01%		-0.07%	
15	-0.05%		-0.11%	
30	-0.02%		-0.14%	
45	0.00%		0.00%	

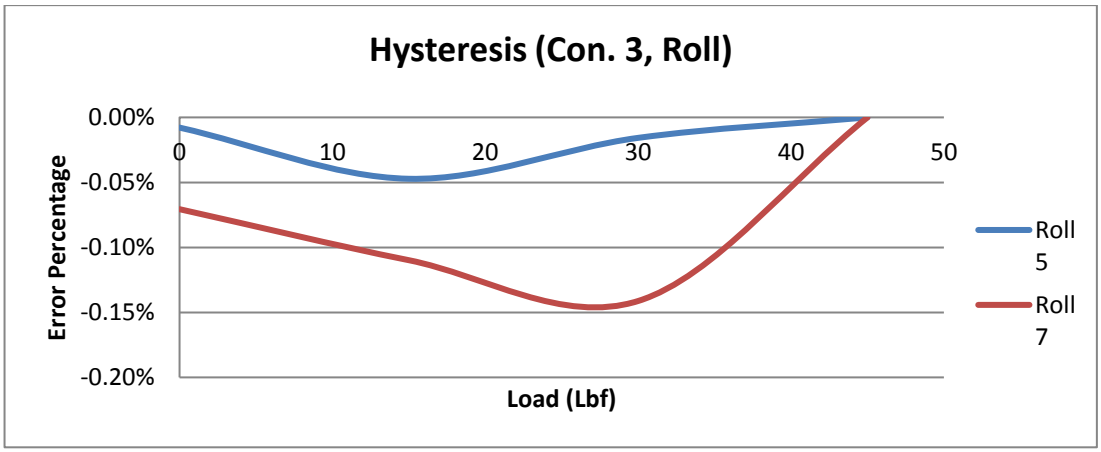

Figure 3.27: Percentage hysteresis graph of roll axis, concept 3

3.6 Summery

Practical issues were considered as the first thing and decisions were taken to prevent those in next step. Number of bonding cycles was effected to the yield of the gauge bonding process. Next design has to be designed to have less number of bonding cycles, ideally one. Bonding strain gauges on curved surface were made grate difficulties in process and in proper bonding as well. Elimination of bonding process difficulties was one of the main considerations of the next design step. During the wiring of strain gauges, problem encountered and damaged the strain gauge solder tabs due to the stiffness of the wires. Usage of less stiff wires and bondable terminals in next stage is recommended to prevent direct soldering of wire to the strain gauge. Bondable terminals consist with two tabs and backing material, which stick to the metal. Wires are to be soldered directly to bondable terminal and bondable terminal connect to strain gauge using less stiff magnet wires.

Table 3.25 contains summery of analysis results. When considered cross sensitivity percentage value, none of the concept was behaved within the required limitations and others were demonstrated huge deviation. Comparatively concept 2 had a lesser value of cross sensitivity percentage. When considered non linearity values, except concept 1 pitch axis sensor channels, all other sensors were behaved well within the requirement. Concept 3 sensor nonlinearity values were comparatively lower than other two. Hysteresis characteristics of the sensors were also lower than one percent and concept 3 had the best performance comparatively. Considering overall results decision was taken to continue with the concept 3 sensor and do modification to achieve cross sensitivity requirement.

Table 3.25: Summery of analysis results

		Maximum percentage value		
		Cross sensitivity	Non linearity	Hysteresis
Concept 1	Pitch	2.40%	-41.36%	0.24%
	Roll	37.72%	-0.84%	-0.35%
Concept 2	Pitch	-20.25%	-0.86%	-0.83%
	Roll	-27.78%	-0.27%	-0.31%
Concept 3	Pitch	55.00%	0.60%(-0.19%)*	- 0.71%(-0.23%)*
	Roll	-16.30%	0.13%	-0.14%

* - Outlier value was not considered and second highest value is taken as the highest non linearity.

4. Final Design

Design concept of final design and how it designed to overcome the drawbacks and practical problems are deeply described in this chapter. Mathematical model of the final design concept is also included in this chapter and it discus how it used to decide the suitable parameter ranges of the sensor. Fabrication of the final design and its test results and analysis of them are also included in this chapter.

4.1 Design concept

Design concept 4 was modeled to overcome recognized drawbacks of the preliminary stage designs. When the time came to concept 4 design space envelop also changed. New design got a smaller envelop than previous and concept of sensor inside the sensor came in to the picture in order to achieve the space requirements. Figure 4.1 shows the solid model of the concept 4 design. Figure 4.1(a) shows the exploded view of the model and Figure 4.1(b) shows the sectional view of the DAFSA concept 4 sensor assembly. Outer sensor screwed to the mounting part and inner sensor was mounted on the outer sensor. The given force is transferred to the sensor using a shaft which is fixed to the inner sensor using a machined thread.

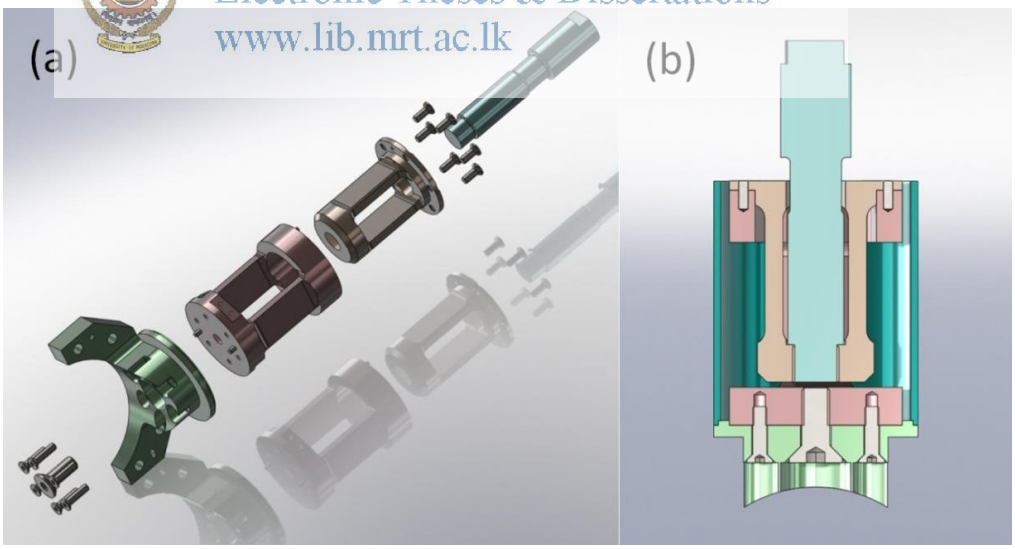

Figure 4.1: Solid modal of concept 4, (a) Explode view of the solid model, (b) Integrated solid model

4.2 Mathematical model

Mathematical model of the design concept 4 was necessary to have in order to optimize beam thickness of the sensor elements and to have an idea of the cross sensitivity behavior of the sensors. Mathematical model were developed to output the strains of the bonding area at each load.

Stress and strain of the beam has following relation while stress remains well below the yield strength of the material [12]. Assuming material is homogeneous.

$$\sigma = \frac{Mz}{I} \quad (10).$$

$$\sigma = E\varepsilon \quad (11).$$

M is the bending moment. z is the distance from the neutral axis to a point of interest. E is the elastic modulus and I is the second moment of area. I must be calculated with respect to the centroidal axis perpendicular to the applied loading. σ is tensile stress and ε is strain of the beam.

Clamped guided beam is a beam which has two beams and connected from both side. That deforms as shown in the Figure 4.2 when load applies to the direction as shown.

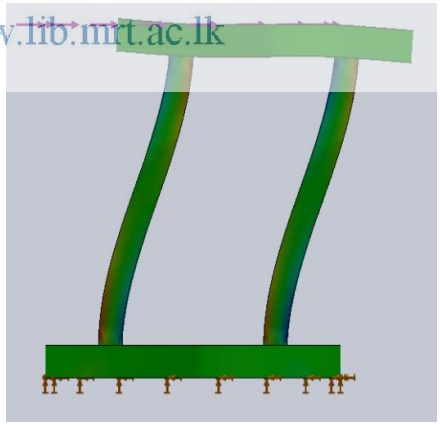

Figure 4.2: Deformed shape of the clamped guided beam when load applied to in direction perpendicular to the width of column.

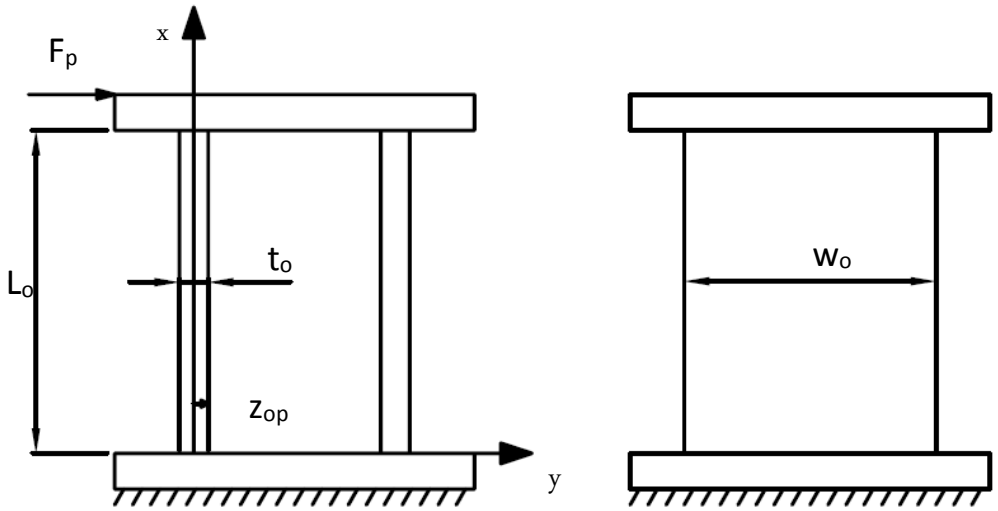

Figure 4.3: Simplified body diagram for mathematical model of outer sensor when pitch load applied

Bending moment distribution along the beam of a clamped guided beam is describing as follows [13]. F is the force applied to the perpendicular to the centroidal axis and L is the length of the beam.

`

$$M = F\left(\frac{L}{2} - x\right) \quad (12).$$

$$M_{x_{op}} = \frac{F_p L_o}{2}\left(\frac{L_o}{2} - x\right) \quad (13).$$

F_p is the force applied for the pitch direction. $M_{x_{op}}$ is bending moment of the outer sensor when applied the pitch load. L_o is the length of the beam of outer sensor. z_{op} is distance to the gauge bonding surface from center axis x. t_o and w_o is outer sensor thickness and width of the beam respectively. Figure 4.3 shows the parameters of the outer sensor.

$$z_{op} = \frac{t_o}{2} \quad (14).$$

$$I_{x_{op}} = \frac{w_o {t_o}^3}{12} \quad (15).$$

$I_{x_{op}}$ is second moment of area of the outer sensor element.

Considering equation (10) and (11)

$$\varepsilon = \frac{Mz}{EI} \quad (16).$$

By substituting (13), (14) and (15) in (16)

$$\varepsilon_{op} = \frac{F_p t_o (L_o - 2x)}{8E \frac{w_o {t_o}^3}{12}} \quad (17).$$

$$\varepsilon_{op} = \frac{3F_p (L_o - 2x)}{2E w_o {t_o}^2} \quad (18).$$

Where ε_{op} is strain on the gauge bonding surface of outer sensor at pitch load.

Clamped guided beam deforms when load applied in the direction which parallel to the width of two beams, as shown in the Figure 4.4.

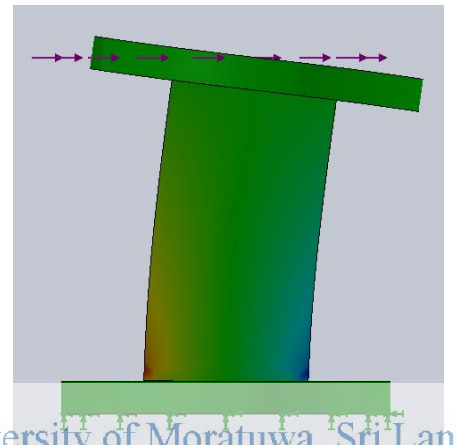

Figure 4.4: Deformed shape of the clamped guided beam when load applied to in direction parallel to the width of column.

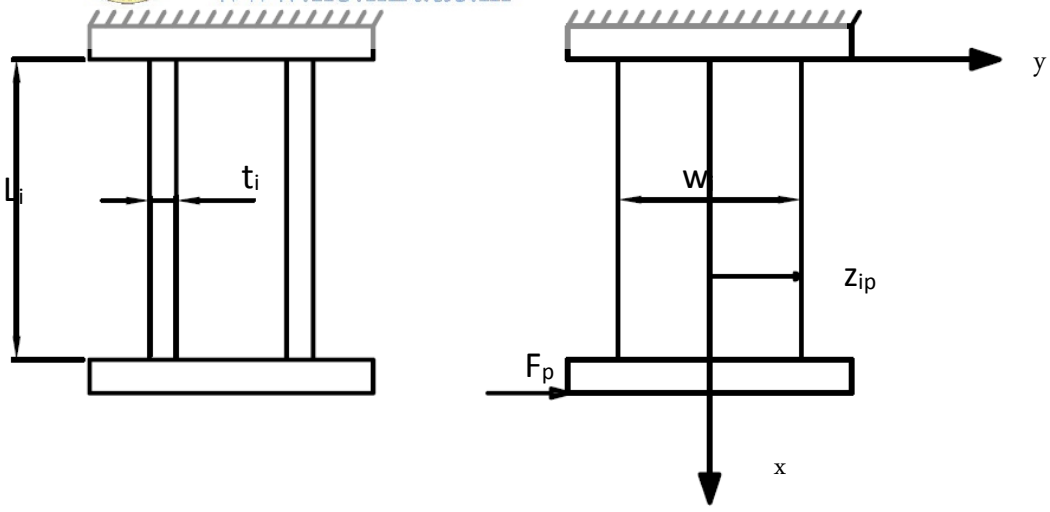

Figure 4.5: Simplified body diagram for mathematical model of inner sensor when pitch load applied

Bending moment distribution along the beam of a cantilevered beam is describing as follows.

$$M = F(L - x) \tag{19}.$$

$$M_{x_{ip}} = \frac{F_p}{2}(L_i - x) \tag{20}.$$

L_i is the length of the column of the inner sensor element. $M_{x_{ip}}$ is bending moment of column of inner sensor element.

$$I_{x_{ip}} = \frac{t_i {w_i}^3}{12} \tag{21}.$$

By substituting (20) and (21) in (16)

$$\varepsilon_{ip} = \frac{F_p(L_i - x)y}{2E\frac{t_i {w_i}^3}{12}} \tag{22}.$$

$$\varepsilon_{ip} = \frac{6F_p(L_i - x)y}{E t_i {w_i}^3} \tag{23}.$$

Where ε_{ip} is strain of the gauge bonding surface of inner sensor when pitch load applied. t_i and w_i are thickness and width of the inner sensor columns respectively.

According to the same above manner it can find strain on the outer element gauge bonding surface and inner element gauge bonding surface when applied the roll load F_r.

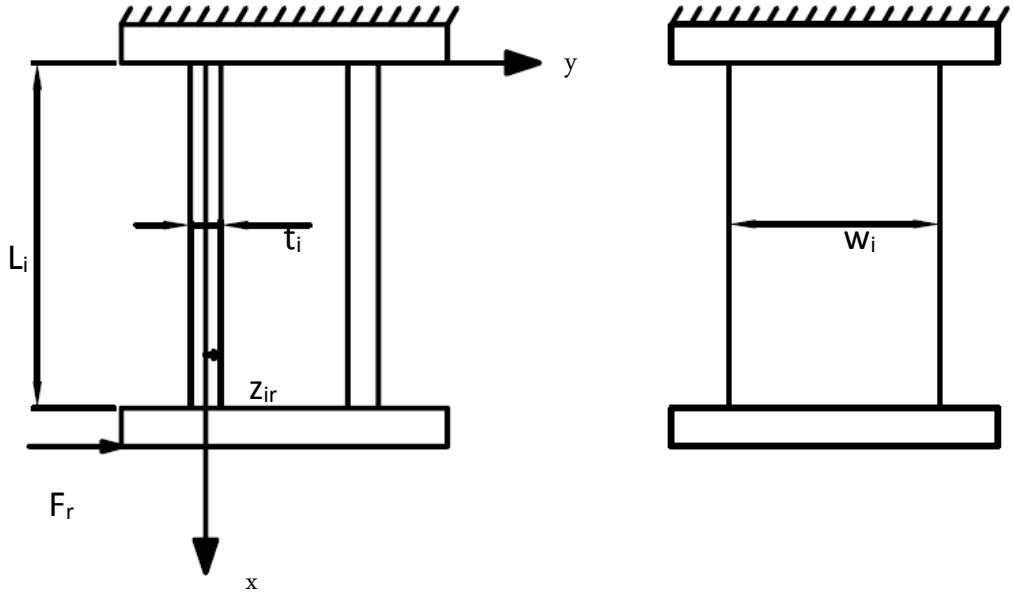

Figure 4.6: Simplified body diagram for mathematical model of inner sensor when roll load applied

$$\varepsilon_{ir} = \frac{3F_r(L_i - 2x)}{2Ew_i{t_i}^2} \quad (24).$$

Where ε_{ir} is strain of the gauge bonding surface of inner sensor when roll load applied

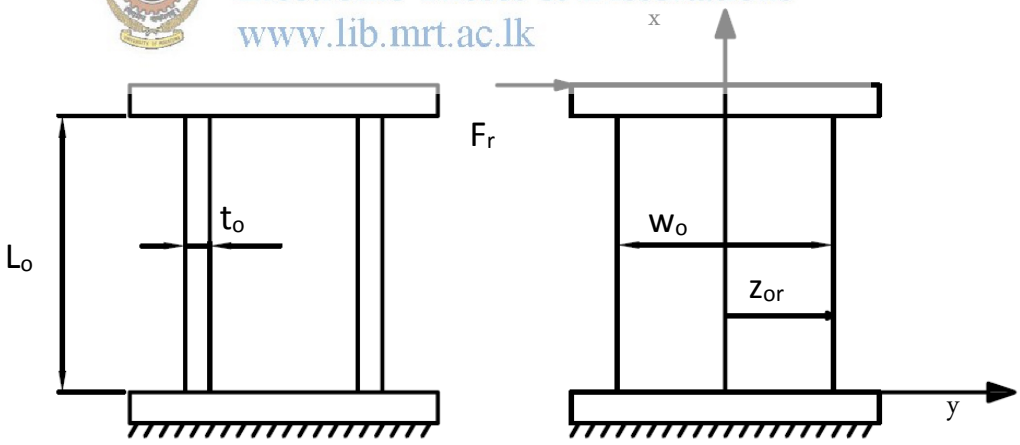

Figure 4.7 Simplified body diagram for mathematical model of outer sensor when roll load applied

$$\varepsilon_{or} = \frac{6F_r(L_o - x)y}{E{t_o}{w_o}^3} \quad (25).$$

Where ε_{or} is strain of the gauge bonding surface of outer sensor when roll load applied.

4.3 Outcomes of the mathematical model

Equation (18) and (24) clearly illustrate, direct strain on the sensor element varies with the length, width, thickness of the beam, x direction distance and the applied force. Maximum strain occurs when x equal to zero and x equal to total length of the beam, but opposite in sign. That means the both ends of the beam having maximum strain. With of the beam and length of the beam can only change within a small rang. Because, those two variables are highly depend on the outer dimension of the sensor and design of it. Thickness of the beam had vary in steps of 0.1 mm and calculate the strain on the bonding surfaces and selected the range of thickness for pitch and roll sensors.

Cross sensitivity strain of the sensor elements describes in equation (23) and (25). It depends on length, width, thickness of the beam and applied load on the sensor. This equation illustrates well that strain not only varies along the longitudinal direction of the beam but also through the width of the beam. Highest strain occurs through the both edge of the beam top surface.

Cross sensitivity reduction had the highest attention of the design concept 4. As described by the equation (23) and (25) cross sensitivity strain inversely proportional to w^3. So, it was clearly identified that by increasing the width of the beam possible to gain low cross sensitivity and it will reduce the direct sensitivity as well. It was decided to degrade the output up to 0.5 mille volts per volts and design was conducted to achieve maximum direct strain of 250 micro strains on the gauging surfaces.

Outer sensor had designed to have beam with (W) of 14.5 mm and length (L) of 31 mm, and they were pre-defined based on the sensor envelop requirements. Only variable which can freely vary was thickness of the beam. As equation (18) figure out beam has same strain along the width of the beam. Figure 4.8 shows the variation of the strain through the longitudinal direction of the beam with the beam thickness. X axis shows the beam length with 0.5 mm variation and y axis shows thickness of the beam it increase with 0.25mm variations and start from 2mm. results were implemented in a excel work sheet and selected the desired thickness range of the beam thickness. Figure 4.9 shows the cross strain variation of the beam with the thickness of it. According to the equation (23) it is visible cross strain varies across the length of the beam as well as across the width of the beam. Cross stress curve was plotted for the line drown in longitudinal direction and 4mm away from the center line of the beam.

Selected thickness range for outer roll sensor was 3.4mm to 4.0mm and for inner sensor 3.8 mm and 4.3 mm. Solid work models were simulated for select the correct beam thickness. Solid works results were end up with results of beam thickness as 3.30 mm outer beam thickness and 3.90 mm inner sensor beam thickness.

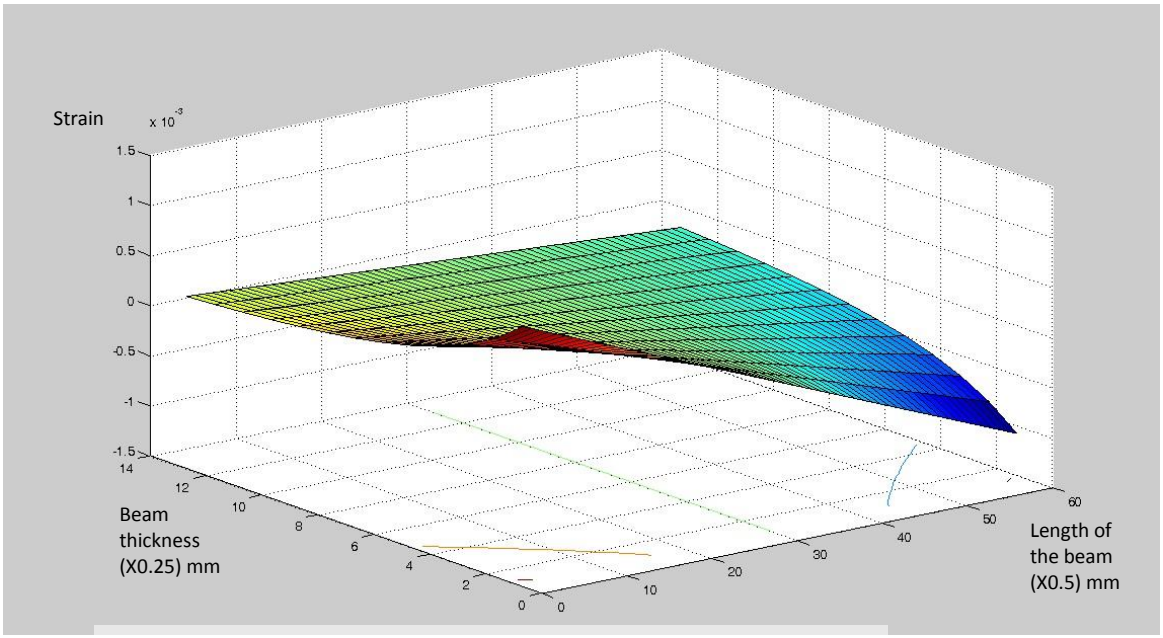

Figure 4.8: Strain variation with length of the beam and thickness of the beam

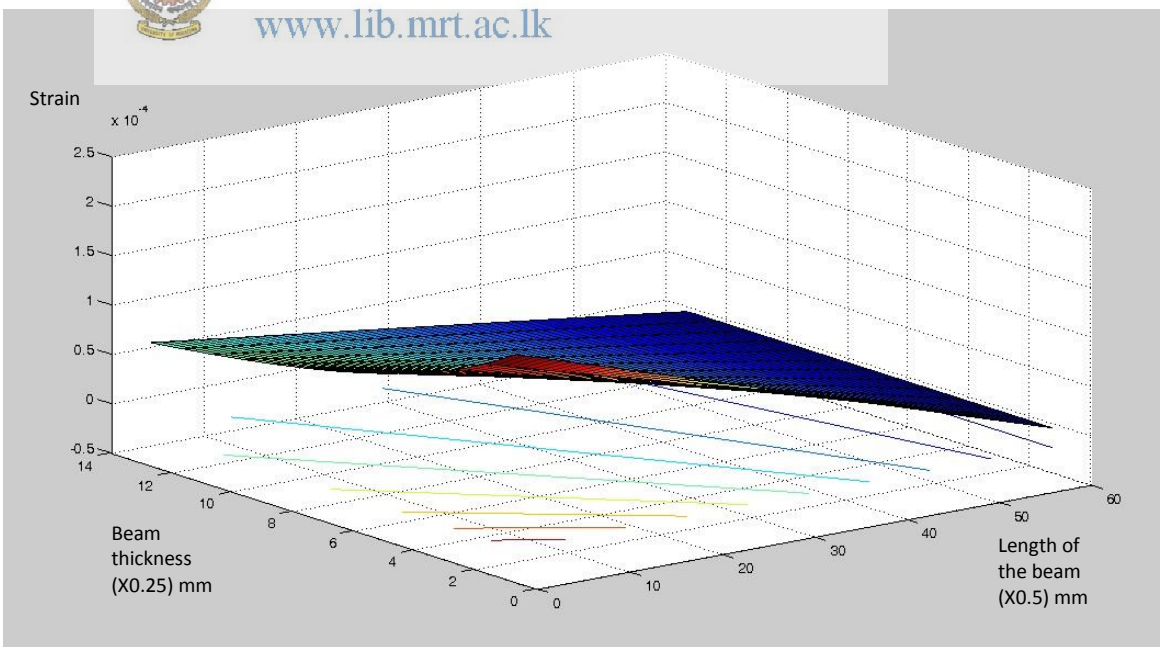

Figure 4.9: Cross strain variation with length of the beam and thickness of the beam

4.4 Fabrications

Fabrication process is almost same as describe in section 3.2. Due to the design changes all 32 strain gages can be bonded in one bonding cycle. Two sensor elements are fabricated separately and assemble just before the wiring of the sensor. But in this design concept gauged only 16 gauges per sensor. Gauges were purchase from Vishay and planned to continue with minimum possible number of strain gauges. As per the plan two Wheatstone bridges were made for one direction sensor and strain gauges were placed where the worst case performance can occurred. As described in the section 4.3 highest strain develop near by the edge of the beams when it came to the cross sensitivity values. Because of that all the strain gauges were placed as much as near to the edge of the column.

Bondable terminals were introduced to the fabrication process and Figure 4.10 shows the way they used in the concept 4. Bondable terminals were bonded to the metal and wires were soldered directly to the terminals. In between the strain gauge and bondable terminal magnet wires were placed with a little bend in order to provide strain relief of the strain gauge.

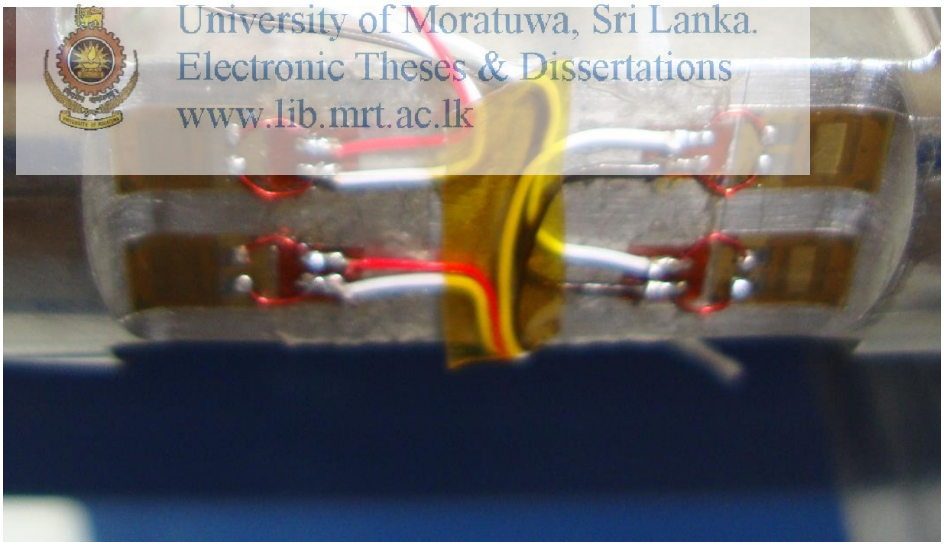

Figure 4.10: Use of bondable terminal in wiring

4.5 Tests and test results

Fabricated DAFSA concept 4 was tested in pitch and roll directions as described in section 2.3. All the test were performed twice to have more reliable data. Table 4.1 and Table 4.2 contains load test data.

Table 4.1: Load test results of concept 4, pitch direction.

Load (lbf)	Output (mV/V)							
	1P		2P		1R		2R	
	1st trial	2nd trial	1st trial	2nd trial	1st trial	2nd trial	1st trial	2nd trial
00	0.0000	0.0000	0.0000	0.0000	0.0000	0.0000	0.0000	0.0000
15	0.1365	0.1366	0.1351	0.1351	-0.0032	-0.0032	0.0028	0.0028
30	0.2737	0.2739	0.2704	0.2701	-0.0067	-0.0064	0.0056	0.0057
45	0.4105	0.4112	0.4055	0.4052	-0.0104	-0.0106	0.0095	0.0085
60	0.5473	0.5478	0.5410	0.5402	-0.0137	-0.0143	0.0117	0.0113
45	0.4110	0.4115	0.4058	0.4055	-0.0132	-0.0132	0.0112	0.0115
30	0.2744	0.2749	0.2706	0.2703	-0.0103	-0.0099	0.0091	0.0087
15	0.1380	0.1381	0.1350	0.1350	-0.0053	-0.0053	0.0048	0.0049
00	0.0000	0.0002	0.0001	0.0000	-0.0001	-0.0001	0.0001	0.0001

Table 4.2: Load test results of concept 4, roll direction.

Load (lbf)	Output (mV/V)							
	1R		2R		1P		2P	
	1st trial	2nd trial	1st trial	2nd trial	1st trial	2nd trial	1st trial	2nd trial
00	0.0000	0.0000	0.0000	0.0000	0.0000	0.0000	0.0000	0.0000
15	-0.1769	-0.1769	-0.1757	-0.1756	0.0025	0.0025	-0.0025	-0.0025
30	-0.3535	-0.3535	-0.3518	-0.3517	0.0060	0.0057	-0.0060	-0.0052
45	-0.5300	-0.5298	-0.5281	-0.5280	0.0085	0.0080	-0.0077	-0.0070
30	-0.3532	-0.3531	-0.3523	-0.3523	0.0064	0.0059	-0.0060	-0.0053
15	-0.1767	-0.1766	-0.1762	-0.1762	0.0039	0.0035	-0.0035	-0.0030
00	-0.0002	-0.0001	-0.0001	-0.0002	0.0002	0.0001	0.0000	0.0002

Based on above load test results, cross sensitivity percentage, Nonlinearity error percentage and hysteresis error percentage was calculated and summarized through Table 4.3 to Table 4.8 below. Graph of the error behavior is below the each error data table.

Table 4.3: Percentage cross sensitivity values of pitch axis, concept 4.

Load (lbf)	percentage of cross sensitivity%			
	1P		2P	
Ascending	1st trial	2nd trial	1st trial	2nd trial
0	0.00%	0.00%	0.00%	0.00%
15	-1.41%	-1.41%	1.42%	1.42%
30	-1.70%	-1.61%	1.71%	1.48%
45	-1.60%	-1.51%	1.46%	1.33%
Descending				
45	-1.60%	-1.51%	1.46%	1.33%
30	-1.81%	-1.67%	1.70%	1.50%
15	-2.21%	-1.98%	1.99%	1.70%
0	0.00%	0.00%	0.00%	0.00%

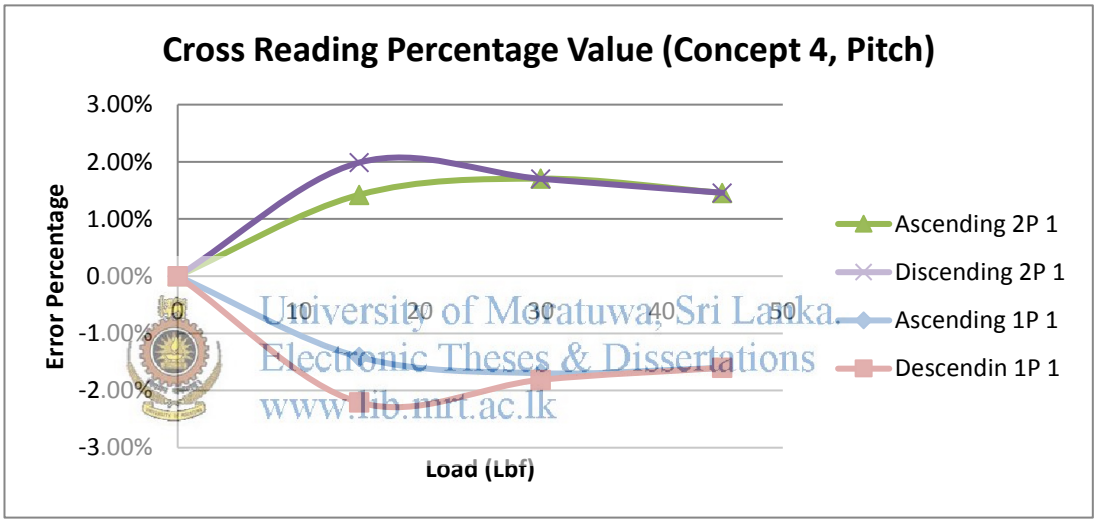

Figure 4.11: Percentage cross sensitivity graph of pitch axis, concept 4.

Table 4.4: Percentage non linearity value of pitch axis, concept 4

Load (lbf)	Non linearity %			
	1P		2P	
Ascending	1st trial	2nd trial	1st trial	2nd trial
0	0.00%	0.00%	0.00%	0.00%
15	-0.06%	-0.06%	-0.03%	0.01%
30	0.01%	0.00%	-0.02%	0.00%
45	0.00%	0.06%	-0.05%	0.01%
60	0.00%	0.00%	0.00%	0.00%
Descending				
60	0.00%	0.00%	0.00%	0.00%
45	0.10%	0.12%	0.01%	0.06%
30	0.14%	0.18%	0.02%	0.04%
15	0.21%	0.21%	-0.05%	-0.01%
0	0.00%	0.04%	0.02%	0.00%

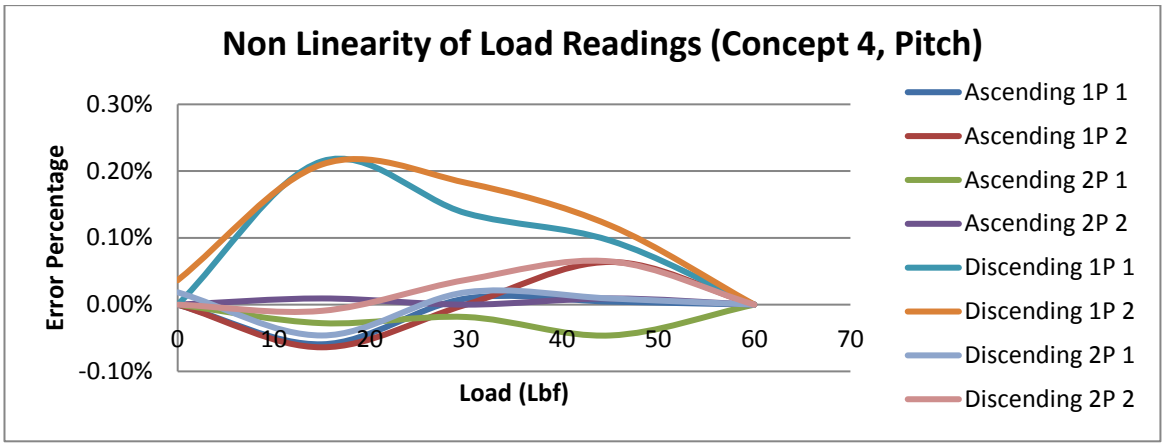

Figure 4.12: Percentage non linearity graph of pitch axis, concept 4

Table 4.5: Percentage hysteresis value of pitch axis, concept 4

Load (lbf)	Hysteresis %			
	1P		2P	
	1st trial	2nd trial	1st trial	2nd trial
0	0.00%	0.04%	0.02%	0.00%
15	0.27%	0.27%	-0.02%	-0.02%
30	0.13%	0.18%	0.04%	0.04%
45	0.09%	0.05%	0.06%	0.06%
60	0.00%	0.00%	0.00%	0.00%

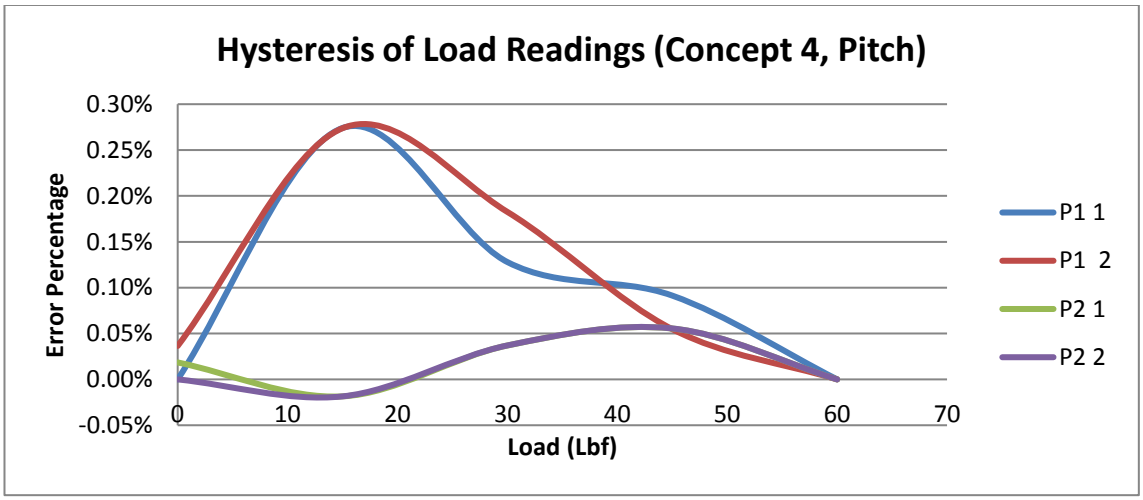

Figure 4.13: Percentage hysteresis graph of pitch axis, concept 4

Table 4.6: Percentage cross sensitivity values of roll axis, concept 4.

Load (lbf)	percentage of cross sensitivity%			
	1R		2R	
Ascending	1st trial	2nd trial	1st trial	2nd trial
0	0.00%	0.00%	0.00%	0.00%
15	-2.34%	-2.34%	2.07%	2.07%
30	-2.45%	-2.34%	2.07%	2.11%
45	-2.53%	-2.58%	2.34%	2.10%
60	-2.50%	-2.61%	2.16%	2.09%
Descending				
60	-2.50%	-2.61%	2.16%	2.09%
45	-3.21%	-3.21%	2.76%	2.84%
30	-3.75%	-3.60%	3.36%	3.22%
15	-3.84%	-3.84%	3.56%	3.63%
0	0.00%	0.00%	0.00%	0.00%

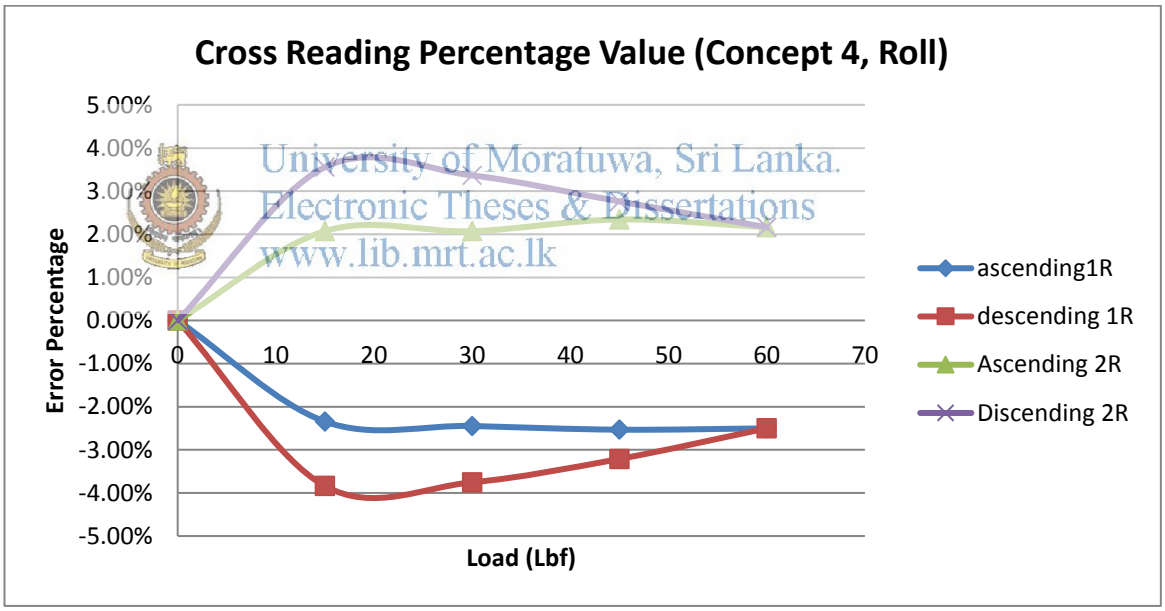

Figure 4.14: Percentage cross sensitivity graph of roll axis, concept 4.

Table 4.7: Percentage non linearity value of roll axis, concept 4.

Load (lbf)	Non linearity %			
	1R		2R	
Ascending	1st trial	2nd trial	1st trial	2nd trial
0	0.00%	0.00%	0.00%	0.00%
15	0.04%	0.06%	-0.06%	-0.08%
30	0.03%	0.06%	-0.05%	-0.06%
45	0.00%	0.00%	0.00%	0.00%
Descending				
45	0.00%	0.00%	0.00%	0.00%
30	-0.03%	-0.02%	0.04%	0.06%
15	0.01%	0.00%	0.03%	0.04%
0	0.04%	0.02%	0.02%	0.04%

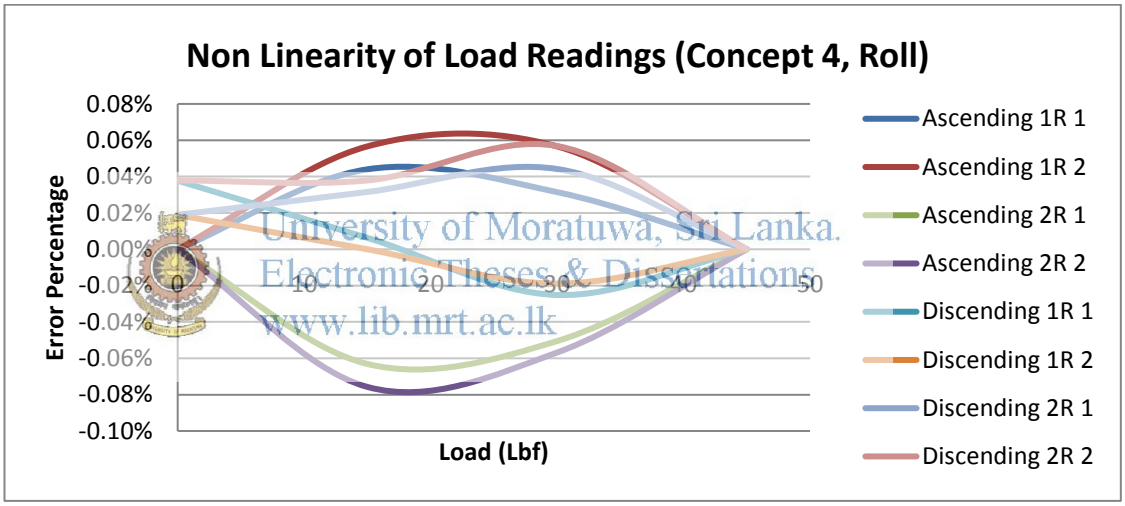

Figure 4.15: Percentage non linearity graph of roll axis, concept 4

Table 4.8: Percentage hysteresis value of roll axis, concept 4

Load (lbf)	Hysteresis %			
	1R		2R	
	1st trial	2nd trial	1st trial	2nd trial
0	0.04%	0.02%	0.02%	0.04%
15	-0.04%	-0.06%	0.09%	0.11%
30	-0.06%	-0.08%	0.09%	0.11%
45	0.00%	0.00%	0.00%	0.00%

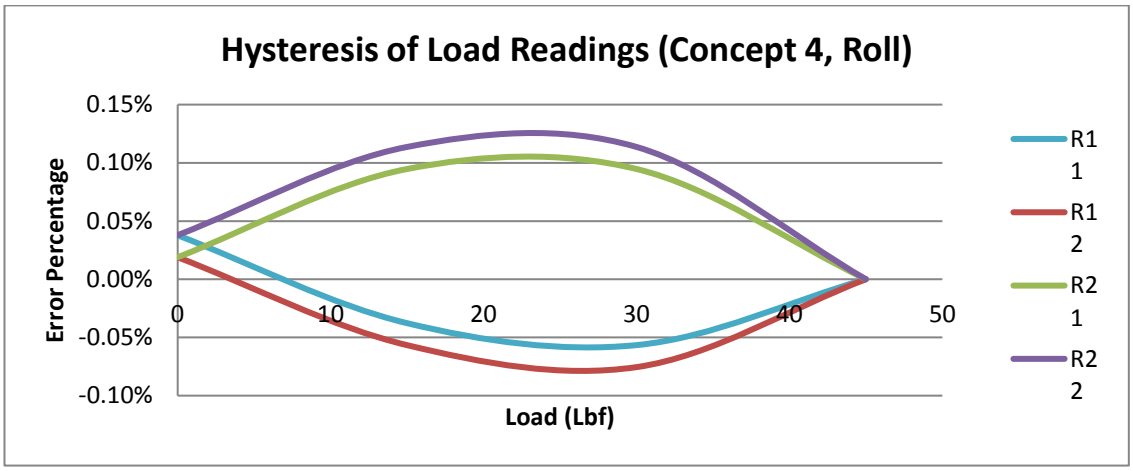

Figure 4.16: Percentage hysteresis graph of roll axis, concept 4

CHAPTER 5

5. Results and Analysis

This chapter concludes all the results of the final design and preliminary designs and further development ideas were also included.

5.1 Final results and analysis

Mathematical model was developed to have an initial beam thickness to start FEA analysis. FEA analysis has proven the mathematical model. Additionally cross torque sensitivity also optimized against the sensor output based on the mathematical model.

Table 5.1 shows the summary of the results comparison of the concept 3 and concept 4. Concept 3 had the best result among preliminary three concepts and concept 4 was developed to overcome the drawbacks identified in concept 3 and to upgrade the functional measurements. One of the concept 4 force sensor pitch channel has undesirable results and those readings made significant difference to the performance indicators of the sensors. Second best performance values are also shown within the brackets in Table 5.1 and outliers were ignored.

Table 5.1: Results summary of concept 4 and concept 3.

		Maximum percentage value		
		Cross sensitivity	Non linearity	Hysteresis
Concept 3	Pitch	55.00%	0.60%(-0.19%)*	- 0.71%(-0.23%)*
	Roll	-16.30%	0.13%	-0.14%
Concept 4	Pitch	-2.21%	0.21%(0.065%)**	0.27 %(0.06%)**
	Roll	-3.84%	0.08%	0.11%
Reduction percentage	Pitch	95.98%	65.79%	73.91%
	Roll	76.44%	38.46%	21.43%

5.2 Conclusion

Functional requirements were fine tuned in the concept 4 design based on the mathematical model and the FEA results. Table 5.1 shows the percentage reductions of all the results achieved through concept 4 design. Non linearity value was reduced by 65.79% and 38.46% pitch and roll directions respectively. Achieved non linearity values are 0.065% in pitch direction and 0.08% in roll direction. Hysteresis also

reduced by 73.91% in pitch direction and 21.43% in roll direction. 0.06% and 0.11% hysteresis values achieved in pitch and roll directions. Cross sensitivity is the major drawback encountered in design concept 3. Concept 4 achieved 2.21% pitch cross sensitivity and 3.84% roll cross sensitivity. Compared to the concept 3 it is 95.98% and 76.44% reductions. As desired cross sensitivity requirement was 2% of the applied load, concept 4 was marginally failed the requirement. All the functional requirements were upgrade in concept 4 design and it was success development for Aerosence technologies (pvt) ltd. Concept 4 dual axis force sensor is a optimized solution in between the cross sensitivity and sensor output.

During the fabrications of preliminary design stage, lots of practical issues were met. Concept 4 design was developed for overcome all of them as well. New design concept allowed to operator to bond all the strain gauges at single cycle of bonding and curing and all the strain gauges were pasted on the external surfaces, so strain gauge bonding was easier than preliminary stage. Strain gauges bonding first pass yield is 100% for all three of concept 4 models. Zero unbalance was another problem encountered during the preliminary design stage. But concept 4 design had no such disadvantage. A concept 4 force sensor meets its functional requirements and it is well developed product for the mass scale manufacturing as well.

Output of the Wheatstone bridge reduced to 0.5 millivolts per volts in order to achieve the cross sensitivity requirement. So it was required more signal amplification. Amplifier amplifies the reading and the noises at the same time, so it was required to have more signal conditioning. That is a drawback identified in the system developed.

Concept 4 design had achieved intended development in all the functional aspects defined in the beginning of the design.

5.3 Further development

Development came up to mile stone and need only fewer adjustments for the concept 4. But there may be any application which need zero cross sensitivity. Concept 5 developed to gain zero cross sensitivity. But there are some rubbing surfaces in the design and with the time it is possible to make a dead zone of the reading due to the wear off of rubbing parts. Dead zone is a zone which has no changes of the output reading while applying the load on the sensor. This is not allowable in aerospace application.

New design concept 5 consists of five basic parts. Two of them are load cells. Figure 5.1(a) illustrates pitch axis load cell and Figure 5.1(b) illustrates roll axis load cell. Major advantage of this design is almost elimination of the cross sensitivity effect. Figure 5.1(d) is a model of load separator. The load separating mechanism separates pitch and roll load effect on the sensing element. While we applying load in one direction load separator apply load on the appropriate sensing element and slips through the grove on other sensing element while eliminating cross sensitivity. Figure 5.1 (e) shows close view of load separating mechanism and Figure 5.1(a) is exploded view of sensor assembly. Strain gages can be pasted on outer side of both columns. Mathematical model of the concept 5 is shown in the Appendix B.

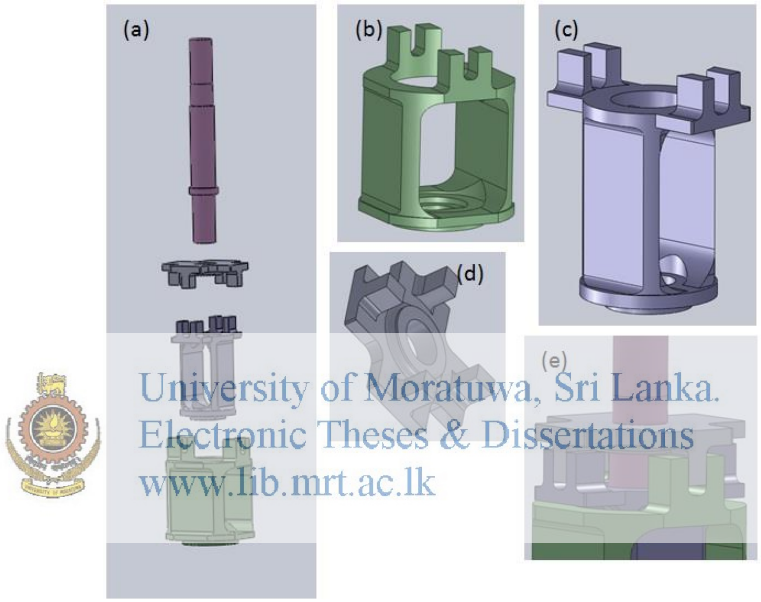

Figure 5.1: Concept 5 design model. (a) Exploded view of sensor concept 5 model without outer casing. (b) Pitch axis load sell in concept 4 design. (c) Roll axis load sell in concept 4 design. (d) Load separator part witch separate effect on sensor parts by roll axis load and pitch axis load. (e) Close view of assembled sensor load separating mechanism

References

[1] J. Fraden, "Handbook of Modern Sensors: Physics, Designs, and Applications," 3rd edition, Springer: New York, 2004, pp. 64-66,325-236.

[2] Y. Sun, B. J. Nelson, " MEMS capacitive force sensors for cellular and flight biomechanics," Biomedical materials, Mar 2007, pp.s16-s22

[3] S. Somlor, A. Schmitz, R.S. Hartanto, S.Sugano, "A prototype force sensing unit for a capacitive-type force-torque sensor," System Integration, 2014, pp. 684-689.

[4] A. A. Barlian, W. T. Park, J. R. Mallon, A. J. Rastegar, and B. L. Pruitt, "Review: Semiconductor Piezoresistance for Microsystems," Proceedings of the IEEE, Vol. 97, No. 3, Mar 2009, pp. 513-552.

[5] W. Hernandez, "Improve the response of a load cell by using optimal filtering," Sensors 2006, Jul 2006, pp. 697-711.

[6] C. Lee , T. Itoh , T. Suga , "Micro machined piezoelectric force sensors based on PZT thin films," IEEE Transactions on Ultrasonics, Ferroelectrics, and Frequency Control , Vol. 43, Issue 4 , Jul. 1996, pp. 553-559.

[7] J. G. Webster, "The measurement, instrumentation, and sensors handbook," 1st edition, CRC Press, December 1998, pp. 23.3-23.7.

[8] R. Pacnik, F. Novak, "A high- sensitivity hydraulic load cell for small kitchen appliances," Sensors 2010, Sep 2010, pp. 8452-8465.

[9] H. C. Smith, "The illustrated guide to aerodynamics," 2nd edition, McGraw-Hill, Mar 1992, pp. 159-160.

[10] I. Moir, and A. Seabridge, "Aircraft systems," 3rd edition, John Wiley & Sons Inc, Jun 2008, pp. 04-10.

[11] R.W. Pratt, "Flight control systems practical issues in design and implementation," Institution of Engineering and Technology, Mar 2000, pp. 06-19.

[12] F. P. Beer, E. R. Johnston, J. T. Dewalt, and D. F. Mazurek "Mechanics of Materials," 5th ed. New York: McGraw-Hill, 2009, pp. 216–217.

[13] R. J. Wood, K-J Cho, and K. Hoffman, "Novel Multi Axis Force Sensor for Micro robotics Applications," Smart Materials and Structures Journal, IOP Science Vol. 18 , Nov 2009, pp7.

Appendix A
Source control drawing of DAFSA

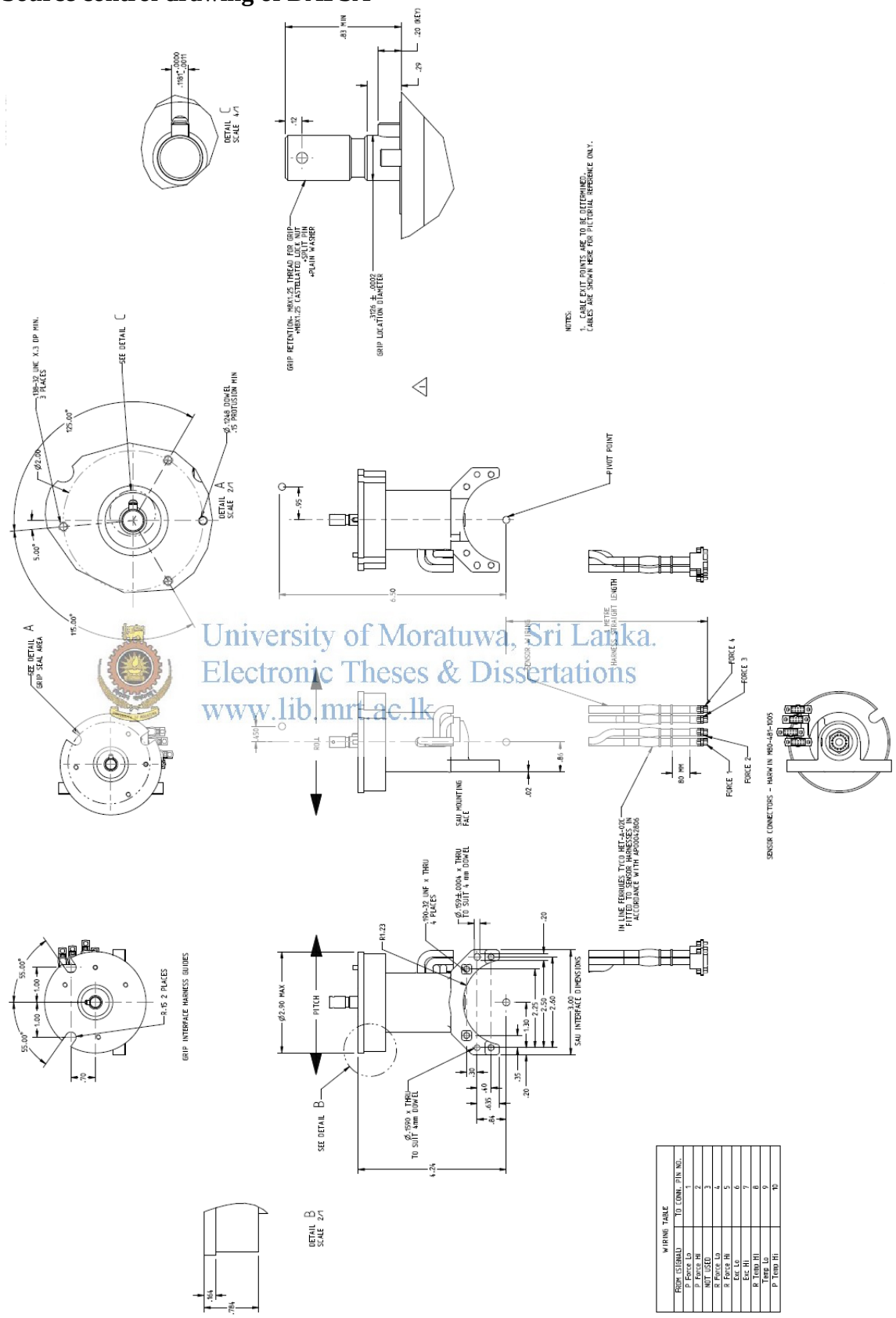

Appendix B
Mathematical model of Concept 5

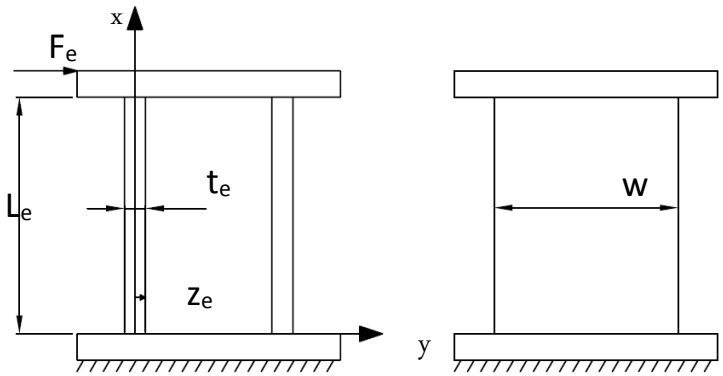

Figure B1. "Concept 5" design simplified sketch of the sensor element.

Stress and strain of the beam has following relation while stress remains well below the yield strength of the material [12]. Assuming material is homogeneous.

$$\sigma = \frac{Mz}{I} \quad \text{(B1).}$$

$$\sigma = E\varepsilon \quad \text{(B2).}$$

M is the bending moment, z is the distance from the neutral axis to a point of interest. E is the elastic modulus and I is the second moment of area. I must be calculated with respect to the centroidal axis perpendicular to the applied loading. σ is tensile stress and ε is strain of the beam.

Bending moment distribution along the beam of a clamped guided beam is describing as follows [13]. f is the force applied to the perpendicular to the centroidal axis and L is the length of the beam.

$$M = f\left(\frac{L}{2} - x\right) \quad \text{(B3).}$$

$$M_{x_e} = f\left(\frac{L_e}{2} - x\right) \quad \text{(B4).}$$

w and t are with and thickness of the beam respectively.

$$f = \frac{F_e}{2} \quad \text{(B5).}$$

F_e is the force element of the total force which effect to the sensor element only.

$$z_e = \frac{t_e}{2} \quad \text{(B6).}$$

Considering equation (B1) and (B2)

$$\varepsilon = \frac{Mz}{EI} \quad \text{(B7).}$$

By substituting (B4), (B5) and (B6) in (B7)

$$\varepsilon_e = \frac{F_e t_e (L_e - 2x)}{8EI_{x_e}} \quad \text{(B8).}$$

I_{x_e} and I_{x_s} are second moment of area of the sensor element and the shaft respectively.

Using (B4) and (B5)

$$M_{x_e} = \frac{F_e}{2}\left(\frac{L_e}{2} - x\right) \quad \text{(B9).}$$

Deflection y at any given point of beam can be explaining using following equation [12].

$$\frac{\partial^2 y}{\partial x^2} = \frac{M_x}{EI} \quad \text{(B10).}$$

Calculating the displacement $y_{(x)_e}$ of the sensor element

$$\frac{\partial^2 y_{(x)_e}}{\partial x^2} = \frac{F_e(L_e - 2x)}{4EI_{x_e}} \quad \text{(B11).}$$

$$y_{(x)_e} = \frac{F_e}{4EI_{x_e}}\left(\frac{L_e x^2}{2} - \frac{x^3}{3}\right) \quad \text{(B12).}$$

Deflection of the extreme end $(x = L_e)$ of the sensor element is.

$$y_{(L)_e} = \frac{F_e L_e^3}{24EI_{x_e}} \quad \text{(B13).}$$

Considering the shaft of the sensor assemble.

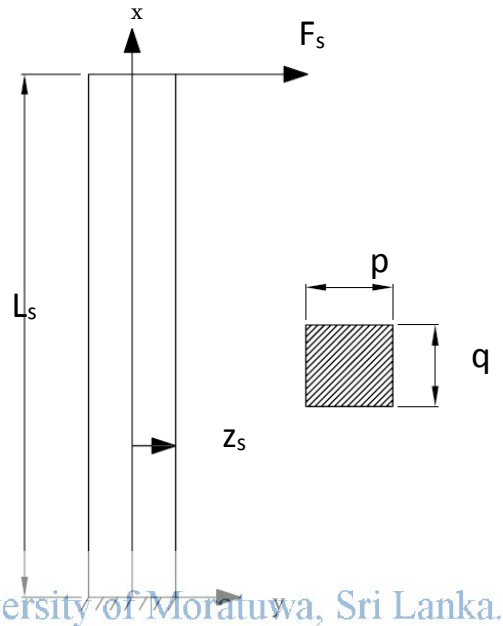

Figure B2. "Concept 5" design simplified sketch of the shaft.

Bending moment distribution along the beam of a cantilevered beam is describing as follows.

$$M = f(L - x) \quad \text{(B14).}$$

$$M_{x_s} = F_s(L_s - x) \quad \text{(B15).}$$

F_s is the force element of the total force which effect to the shaft only.

Substituting (B15) in (B10)

$$\frac{\partial^2 y_{(x)_s}}{\partial x^2} = \frac{F_s(L_s - x)}{EI_{x_s}} \quad \text{(B16).}$$

To calculate the displacement $y_{(x)_s}$ of shaft

$$y_{(x)_s} = \frac{F_s}{EI_{x_s}}\left(\frac{L_s x^2}{2} - \frac{x^3}{6}\right) \quad \text{(B17).}$$

Deflection of the extreme end ($x = L_s$) of the shaft

$$y_{(L)_s} = \frac{F_s L_s^3}{3EI_{x_s}} \quad \text{(B18).}$$

At contacted point $L_s = L_e$ and contacted point displacement $y_{(L)_e}$ of the sensor element and displacement $y_{(L)_s}$ of the shaft should be same.

Using equations (B13) and (B18)

$$\frac{F_s}{I_{x_s}} = \frac{F_e}{8I_{x_e}} \quad \text{(B19).}$$

F is the total force acting on the pitch or roll direction.

$$F_s + F_e = F \quad \text{(B20).}$$

By substituting F_s from (B19) in (B20)

$$F_e = \frac{8FI_{x_e}}{I_{x_s} + 8I_{x_e}} \quad \text{(B21).}$$

By substituting F_e in (B8)

$$\varepsilon_e = \frac{Ft_e(L_e - 2x)}{E(I_{x_s} + 8I_{x_e})} \quad \text{(B22).}$$

$$I_{x_e} = \frac{wt^3}{12} \quad \text{(B23).}$$

$$I_{x_s} = \frac{qp^3}{12} \quad \text{(B24).}$$

$$\varepsilon_e = \frac{12Ft_e(L_e - 2x)}{E(qp^3 + 8wt^3)} \quad \text{(B25).}$$

q and p are with and thickness of the shaft respectively. Using the equation (B25) it is possible to select the p, q, w, t and L_e which give required strain at the total force.

`